

Exceptions to the Ratchet Principle in active and passive stochastic dynamics

Jessica Metzger,¹ Sunghan Ro,^{2,1} and Julien Tailleur¹

¹*Department of Physics, Massachusetts Institute of Technology, Cambridge, Massachusetts 02139, USA*

²*Department of Physics, Harvard University, Cambridge, Massachusetts 02138, USA*

(Dated: March 18, 2025)

The “ratchet principle” asserts that non-equilibrium systems which violate parity symmetry generically exhibit steady-state currents. As recently shown, there are exceptions to this principle, due to the existence of hidden time-reversal symmetry or bulk momentum conservation. For underdamped and overdamped Brownian dynamics, we show how thermal fluctuations cannot power the momentum sources required to sustain steady ratchet currents, even when time-reversal symmetry is broken due to an inhomogeneous temperature field. While Active Brownian and Run-and-Tumble particles display interaction-induced ratchet currents in asymmetric activity landscapes, we show that this is not the case for Active Ornstein Uhlenbeck particles: not all inhomogeneous active fluctuations lead to net momentum sources. For each of the systems considered in this article, we numerically test for the emergence of interaction-induced ratchet currents. We then characterize time-reversal (as)symmetry in position space using a combination of path-integral and operator methods. When the existence of effective momentum conservation is ruled out, we develop perturbation theories to characterize the onset of interaction-induced currents.

CONTENTS

I. Introduction	1	A. Numerics and phenomenology	15
II. Underdamped Passive Brownian Particles	2	B. Time-reversal symmetry	15
A. Numerics and phenomenology	3	C. Momentum conservation	16
B. Time-reversal Symmetry	3	D. Summary	17
C. Bulk steady-state momentum conservation	4	VI. Discussion and Conclusion	17
D. Summary	5	A. Simulation details	17
III. Overdamped Passive Brownian Particles	5	1. Fig. 1	17
A. Numerics and phenomenology	5	2. Underdamped Passive Brownian Particles (Fig. 2)	17
B. Time-reversal symmetry	5	3. Overdamped Passive Brownian Particles (Figs. 3-4)	18
1. TRS at the trajectory level	6	4. Active Brownian and Run-and-Tumble Particles (Figs. 5-6, 8)	18
2. TRS at the operator level	6	5. Active Ornstein Uhlenbeck Particles (Fig. 7)	18
3. Interaction-induced TRS violation	7	B. EPR for interacting U-PBPs in temperature fields	19
C. Effective momentum conservation	7	C. EPR for PBPs	20
D. Emergence of interaction-induced current	8	1. TRS of non-interacting PBPs	20
1. A single particle in potential, temperature, and mobility fields	8	2. EPR for interacting PBPs	21
2. Perturbation theory	8	D. Exact solution for non-interacting 1d RTPs	22
E. Summary	9	E. EPR of interacting AOUPs in activity landscapes	23
IV. Active-Brownian and Run-and-Tumble Particles	9	References	25
A. Numerics and phenomenology	10		
B. Time-reversal symmetry	10		
1. TRS at the trajectory level for 1d RTPs	11		
2. RTPs and ABPs in d dimensions	12		
3. Interaction-induced TRS violations	12		
C. Momentum sources	13		
D. Interaction-induced current	13		
1. Leading-order ratchet current for ABPs and RTPs in d dimensions	13		
2. Run-and-Tumble Particles in 1D	14		
E. Summary	14		
V. Active Ornstein-Uhlenbeck Particles	15		

I. INTRODUCTION

The “Ratchet Principle” states that the violation of time-reversal symmetry (TRS) and parity symmetry generically leads to the emergence of steady-state currents [1]. Its name stems from studies by Smoluchowski, Feynman and others on the rectification of fluctuations

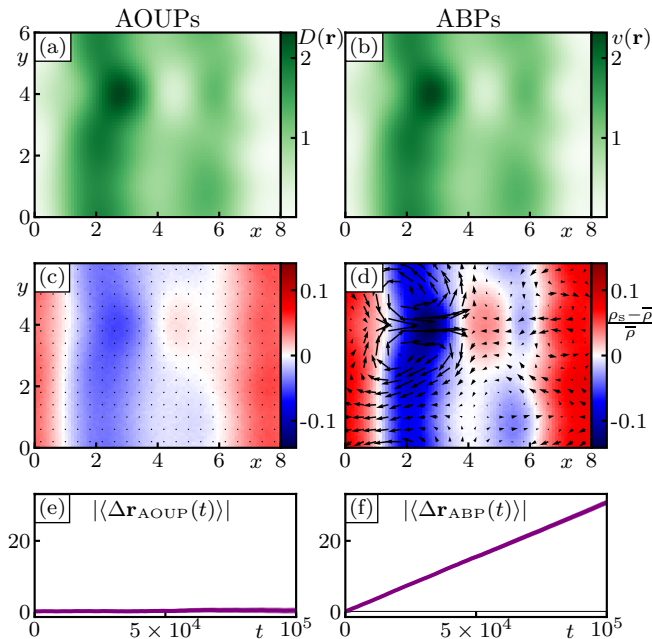


FIG. 1. Interaction-induced currents are observed in ABPs [(b), (d), (f)] in spatially inhomogeneous activity, but not in AOUPs [(a), (c), (e)]. In panels (a)-(b), we show the spatially-varying self-propulsion speed $v(\mathbf{r})$ and diffusivity $D(r)$. In (c)-(d), we show the steady-state density (colored background) and current field (arrows) for AOUPs and ABPs respectively, in the presence of periodic boundary conditions. In panels (e) and (f), we show the average displacement per particle. Simulation details are provided in Appendix A 1.

into steady motion using ratchet-like mechanisms [2, 3]. Ratchets have found applications in a broad range of topics ranging from the motion of molecular motors [2, 4–10] to the rectification of bacterial suspensions [11, 12] and have been proposed as a mechanism to power nonequilibrium microscopic motors [13, 14]. More broadly, they emerge whenever noise and damping do not satisfy a fluctuation-dissipation theorem [15, 16] and are thus ubiquitous in active matter [12, 17–36].

Interestingly, exceptions to the ratchet principle have been reported in systems with spatially varying fluctuation sources. Overdamped passive Brownian particles (PBPs) in an inhomogeneous asymmetric temperature field indeed reach a flux-free steady state in the absence of an external potential [37, 38]. In active matter, run-and-tumble particles (RTPs) and active Brownian particles (ABPs) with spatially varying activity also do not exhibit steady-state currents [39–41], a result that has been generalized to active Ornstein-Uhlenbeck particles (AOUPs) [26]. We note that some of these ratchet exceptions appear fragile. For instance, introducing interactions [42], translational diffusion [43], or a *symmetric* external potential [18] into a system of ABPs with asymmetric activity landscape all lead to the emergence of ratchet currents. Until recently, what controls the exist-

tence of ratchet exceptions had remained elusive.

In our companion Letter [44], we filled this gap and showed how the existence of the aforementioned ratchet exceptions can be rationalized by amending the ratchet principle. For the stochastic systems discussed above, the emergence of ratchet currents was shown to require three conditions, not two: the lack of time-reversal symmetry and of parity symmetry, as expected, but also the existence of net momentum sources. Our results were illustrated by contrasting overdamped PBPs on the one hand, and RTPs and ABPs on the other hand.

In this article, we study these systems separately for their own sake, detailing all relevant methods, and show how the phenomenology of AOUPs and underdamped PBPs (U-PBPs) can also be analyzed within the same framework. Our results not only show how to extend our results beyond the cases considered in [44], they also reveal that the fragility of ratchet exceptions is a subtle question. As illustrated in Fig. 1, interactions indeed do not suffice to induce currents in AOUPs with spatially varying activities, at odd with the ABP result. Interactions and activity are thus not sufficient to induce ratchet currents. We consider underdamped PBPs in Section II, overdamped PBPs in Section III, ABPs and RTPs in Section IV, and AOUPs in Section V. In each section, we first discuss the existence of TRS and then show how, when TRS is violated, currents only emerge when there is no effective momentum-conservation in the bulk. Our results are summarized in Table I. All numerical methods are detailed in appendix A.

II. UNDERDAMPED PASSIVE BROWNIAN PARTICLES

We begin by considering U-PBPs, whose positions \mathbf{r}_i and momenta \mathbf{p}_i evolve according to:

$$\dot{\mathbf{r}}_i = \mathbf{p}_i \quad (1)$$

$$\dot{\mathbf{p}}_i = -\gamma\mathbf{p}_i - \sum_j \nabla U_{\text{int}}(\mathbf{r}_i - \mathbf{r}_j) + \sqrt{2\gamma T(\mathbf{r}_i)}\boldsymbol{\eta}_i. \quad (2)$$

Here the $\{\boldsymbol{\eta}_i(t)\}$ are centered Gaussian white noises that satisfy $\langle \eta_{i,\mu}(t)\eta_{j,\nu}(t') \rangle = \delta_{ij}\delta_{\mu\nu}\delta(t-t')$, with i and j being particle indices, and μ and ν being spatial indices. While our results hold for general potential U_{int} , in this article we use

$$U_{\text{int}}(\mathbf{r}) = \frac{\varepsilon\sigma}{2} \left(1 - \frac{|\mathbf{r}|}{\sigma}\right)^2 \Theta(\sigma - |\mathbf{r}|), \quad (3)$$

where Θ is the Heaviside function. We denote by $\mathbf{f}_{\text{int}}(\mathbf{r}) = -\nabla U_{\text{int}}$ the corresponding interparticle force.

We define the fluctuating phase-space density as

$$\hat{\psi}(\mathbf{r}, \mathbf{p}, t) \equiv \sum_i \delta[\mathbf{r} - \mathbf{r}_i(t)]\delta[\mathbf{p} - \mathbf{p}_i(t)] \quad (4)$$

System	Spatially varying fluctuation source	Interactions	Time-reversal symmetry	Effective momentum conservation	Ratchet current
Underdamped Passive Brownian Particles (U-PBPs)	Temperature			✓	
		✓		✓	
Overdamped Passive Brownian Particles (PBPs)	Temperature		✓	✓	
		✓		✓	
Active Brownian/Run-and-Tumble Particles (ABPs/RTPs)	Activity		✓		
		✓			✓
Active Ornstein-Uhlenbeck Particles (AOUPs)	Activity			✓	
		✓		✓	

TABLE I. Exceptions to the ratchet principle include Underdamped Passive Brownian Particles (U-PBPs) and Overdamped Passive Brownian Particles (PBPs) in spatially-varying temperature fields; along with Active Brownian Particles (ABPs), Run-and-Tumble Particles (RTPs), and Active Ornstein-Uhlenbeck Particles (AOUPs) with spatially-varying activity. A ratchet current is prevented in these systems either by a hidden time-reversal symmetry (TRS) or a bulk momentum conservation. In ABPs and RTPs, a ratchet current is induced by adding a symmetric pairwise interaction potential U_{int} between particles, since this destroys any form of TRS or momentum-conservation in the system. (In Section III D, we show that this is also the case for PBPs with time-discretization $\alpha \in (0, 1)$, where T loses the meaning of a temperature.)

along with its average over noise realizations, $\psi(\mathbf{r}, \mathbf{p}, t) \equiv \langle \hat{\psi}(\mathbf{r}, \mathbf{p}, t) \rangle$. Using Itô calculus [45], we convert Eqs. (1)-(2) to:

$$\begin{aligned} \dot{\psi}(\mathbf{r}, \mathbf{p}, t) = & -\nabla \cdot [\mathbf{p}\psi] + \nabla_{\mathbf{p}} \cdot \left[\gamma T(\mathbf{r}) \nabla_{\mathbf{p}} \psi + \gamma \mathbf{p}\psi \right. \\ & \left. + \int d^d \mathbf{r}' d^d \mathbf{p}' \nabla U_{\text{int}}(\mathbf{r} - \mathbf{r}') \langle \hat{\psi}(\mathbf{r}, \mathbf{p}) \hat{\psi}(\mathbf{r}', \mathbf{p}') \rangle \right]. \end{aligned} \quad (5)$$

We note that, unlike in the overdamped case, there is no ambiguity about where $T(\mathbf{r})$ enters in Eq. (5) since it commutes with $\nabla_{\mathbf{p}}$. The overdamped ($\gamma \rightarrow \infty$) limit of these dynamics corresponds to the Itô time-discretization of overdamped PBPs [38], which we study in Sec. III along with more general discretization schemes.

As we show below, non-uniform temperatures never lead to ratchets currents for U-PBPs, both in the non-interacting and interacting cases. We first show this numerically in Sec. II A. We rule out TRS as a possible explanation in Sec. II B, since U-PBPs with inhomogeneous temperatures are irreversible both in the presence and in the absence of interactions. Finally, we show in Sec. II C that the lack of ratchet currents is due to an effective bulk momentum conservation in the steady state that arises from the existence of a stress tensor.

A. Numerics and phenomenology

We report in Fig. 2 the results of particle-based simulations of U-PBPs in two space dimensions in the temperature landscape shown in Fig. 2(a). We consider systems both with and without pairwise repulsive interactions. The qualitative difference with systems in thermal equilibrium can be seen in the steady-state density shown in

Fig 2(b): In the presence of a temperature field $T(\mathbf{r})$, the damping γ plays a thermodynamic role and the density profile of non-interacting U-PBPs differs from its overdamped limit $\rho(\mathbf{r}) \propto 1/T(\mathbf{r})$. Yet, Fig. 2(c) shows that no current is observed for U-PBPs, even in the presence of interactions.

B. Time-reversal Symmetry

For U-PBPs, TRS can be immediately ruled out as an explanation for the lack of steady currents. Indeed, U-PBPs already exhibit a non-zero entropy production rate (EPR) in the non-interacting limit with spatially varying $T(\mathbf{r})$ [46]. To compute the EPR in the interacting case, we start from the definition:

$$\sigma = \lim_{t_f \rightarrow \infty} \frac{1}{t_f} \left\langle \ln \left[\frac{\mathbb{P}[\{\mathbf{r}_i(t)\} | \{\mathbf{r}_i(0), \dot{\mathbf{r}}_i(0)\}]}{\mathbb{P}[\{\mathbf{r}_i^R(t)\} | \{\mathbf{r}_i^R(0), \dot{\mathbf{r}}_i^R(0)\}]} \right] \right\rangle. \quad (6)$$

where $\{\mathbf{r}_i^R(t)\}$ is the time-reverse of $\{\mathbf{r}_i(t)\}$, defined as

$$\mathbf{r}_i^R(t) = \mathbf{r}_i(t_f - t). \quad (7)$$

In Appendix B, we show how to compute σ using a Stratonovich time discretization of Eqs. (1)-(2). One can then define a fluctuating EPR density field $\hat{\sigma}(\mathbf{r})$ such that $\int d^d \mathbf{r} \langle \hat{\sigma}(\mathbf{r}) \rangle = \sigma$, which reads:

$$\hat{\sigma}(\mathbf{r}) = \sum_i \frac{\delta(\mathbf{r} - \mathbf{r}_i)}{T(\mathbf{r}_i)} \dot{\mathbf{r}}_i \cdot \left[\sum_j \mathbf{f}_{\text{int}}(\mathbf{r}_i - \mathbf{r}_j) - \ddot{\mathbf{r}}_i \right]. \quad (8)$$

The EPR is non-vanishing even in the non-interacting limit, $\mathbf{f}_{\text{int}} = 0$, in agreement with [46]. Equation (8) reveals that interactions introduce new mechanisms for entropy production. As we show below, interaction-induced

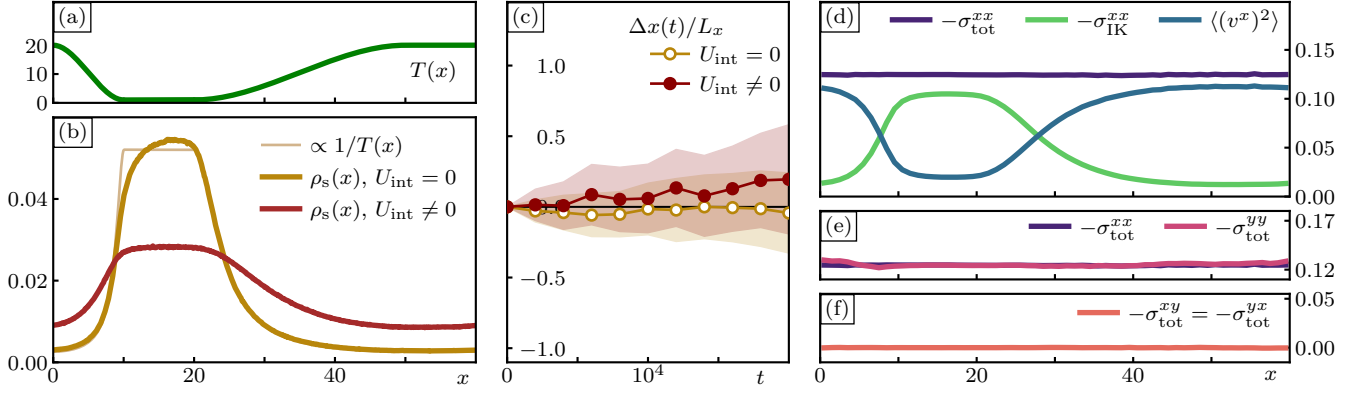


FIG. 2. **Ratchet currents are prevented in a two-dimensional system of U-PBPs by an emergent bulk momentum conservation.** (a) The temperature landscape $T(x)$ used in simulations. (b) The steady-state density distribution of U-PBPs both without (gold) and with (dark red) interactions. The density in the $\gamma \rightarrow \infty$ limit, $\propto 1/T(x)$, is shown for reference (thin tan line). (c) Directly measuring the net particle displacement over time, both without and with interactions, reveals the absence of ratchet current. (d) In the steady state, variations of the momentum flux (blue) are balanced by those of the Irving-Kirkwood stress (green), resulting in a homogeneous pressure σ_{tot}^{xx} and preventing the emergence of a steady current. (e) The (y, y) component of the stress tensor, σ_{tot}^{yy} , varies along x , unlike σ_{tot}^{xx} . It is, however, constant along y by symmetry, thus generating no current. (f) Off-diagonal components of the stress vanish. Simulation details are provided in Appendix A 2.

irreversibility will prove generic in all systems considered in this article.

C. Bulk steady-state momentum conservation

To understand the lack of ratchet currents in U-PBPs, we marginalize Eq. (5) over momentum variables. To do so, we define the fluctuating density $\hat{\rho}$, momentum $\hat{\mathbf{P}}$, and ‘nematic’ order $\hat{\mathbf{Q}}$ fields as

$$\hat{\rho}(\mathbf{r}) \equiv \sum_i \delta(\mathbf{r} - \mathbf{r}_i) = \int d^d \mathbf{p} \hat{\psi}(\mathbf{r}, \mathbf{p}) \quad (9)$$

$$\hat{\mathbf{P}}(\mathbf{r}) \equiv \sum_i \mathbf{p}_i \delta(\mathbf{r} - \mathbf{r}_i) = \int d^d \mathbf{p} \hat{\psi}(\mathbf{r}, \mathbf{p}) \mathbf{p} \quad (10)$$

$$\begin{aligned} \hat{\mathbf{Q}}(\mathbf{r}) &\equiv \sum_i \left(\mathbf{p}_i \otimes \mathbf{p}_i - \mathbb{I} T(\mathbf{r}_i) \right) \delta(\mathbf{r} - \mathbf{r}_i) \quad (11) \\ &= \int d^d \mathbf{p} \hat{\psi}(\mathbf{r}, \mathbf{p}) (\mathbf{p} \otimes \mathbf{p} - \mathbb{I} T(\mathbf{r})) . \end{aligned}$$

We denote their averages as $\rho = \langle \hat{\rho} \rangle$, $\mathbf{P} = \langle \hat{\mathbf{P}} \rangle$, and $\mathbf{Q} = \langle \hat{\mathbf{Q}} \rangle$, respectively.

Integrating Eq. (5) over \mathbf{p} then leads to

$$\dot{\rho} = -\nabla \cdot \mathbf{P} , \quad (12)$$

which shows that, since the particle mass has been taken to unity, momentum density and particles flux coincide. Multiplying Eq. (5) by \mathbf{p} and integrating over \mathbf{p} then leads to

$$\begin{aligned} \dot{\mathbf{P}} &= -\nabla \cdot [\mathbf{Q} + \mathbb{I} \rho T] \\ &\quad - \int d^d \mathbf{r}' \nabla U_{\text{int}}(\mathbf{r} - \mathbf{r}') \langle \hat{\rho}(\mathbf{r}) \hat{\rho}(\mathbf{r}') \rangle - \gamma \mathbf{P} . \quad (13) \end{aligned}$$

In the steady state, $\dot{\mathbf{P}} = 0$, and, using $\mathbf{J} = \mathbf{P}$, we find that

$$\mathbf{J} = -\nabla \cdot \frac{\mathbf{Q} + \mathbb{I} \rho T - \sigma_{\text{IK}}}{\gamma} \equiv \nabla \cdot \frac{\sigma_{\text{tot}}}{\gamma} , \quad (14)$$

where we have absorbed the interaction term into the Irving-Kirkwood stress tensor that satisfies [47]

$$\nabla \cdot \sigma_{\text{IK}} = - \int d^d \mathbf{r}' \nabla U_{\text{int}}(\mathbf{r} - \mathbf{r}') \langle \hat{\rho}(\mathbf{r}) \hat{\rho}(\mathbf{r}') \rangle . \quad (15)$$

Let us now show that Eq. (14) implies the lack of a steady current field. We first note that, using periodic boundary conditions, it implies that

$$\int d^d \mathbf{r} \mathbf{J}(\mathbf{r}) = 0 . \quad (16)$$

Then, Eq. (14) tells us that \mathbf{J} , which is divergence-free in the steady state, must also be curl-free. It is thus a Harmonic vector field and its components are harmonic functions [48]. For periodic boundary conditions, the only harmonic functions are constants so that $J_\alpha(\mathbf{r}) = J_\alpha^0$. Equation (16) then imposes that $J_\alpha^0 = 0$. We thus conclude that, whenever $\mathbf{J}(\mathbf{r})$ can be written as the divergence of a tensor field, it vanishes everywhere in the steady state.

All in all, the fact that the temperature inhomogeneities have a momentum conserving nature, i.e. they enter the evolution of the momentum field \mathbf{P} as $-\nabla \cdot [\mathbf{Q} + \mathbb{I} \rho T]$, enforces that \mathbf{J} vanishes in the steady state. The lack of momentum sources thus prevents the driving of a steady-state current. Note that, for U-PBPs in the temperature field shown in Fig. 2a, we not only have that $\nabla \cdot \sigma_{\text{tot}}$ vanishes, but also that all contributions

vanish separately by symmetry: As shown in Fig. 2c-e, $\partial_x \sigma_{\text{tot}}^{xx} = \partial_y \sigma_{\text{tot}}^{xy} = \partial_x \sigma_{\text{tot}}^{yx} = \partial_y \sigma_{\text{tot}}^{yy} = 0$. We note, however that σ_{tot}^{yy} varies with respect to x , as shown in Fig. 2e, which is inconsequential for the production of currents.

D. Summary

While U-PBPs in spatially-varying temperature fields lack TRS, a ratchet current is prevented by the existence of a generalized stress tensor that enforces bulk momentum conservation. This makes U-PBPs a genuine exception to the ratchet principle.

III. OVERDAMPED PASSIVE BROWNIAN PARTICLES

Let us now consider overdamped PBPs in a temperature field. In d space dimensions, their dynamics read

$$\dot{\mathbf{r}}_i(t) \stackrel{\alpha}{=} - \sum_{j=1}^N \nabla U_{\text{int}}(\mathbf{r}_i - \mathbf{r}_j) + \sqrt{2T(\mathbf{r}_i)} \boldsymbol{\eta}_i(t), \quad (17)$$

where we have taken the mobility to be unity. The symbol $\stackrel{\alpha}{=}$ reminds us that Eq. (17) is only well defined once its time discretization is specified. Introducing a time step Δt and a discretized time $t_k = k\Delta t$, the displacement $\Delta \mathbf{r}_i^k = \mathbf{r}_i^{k+1} - \mathbf{r}_i^k$ of particle i between times t_k and t_{k+1} is then given by:

$$\Delta \mathbf{r}_i^k = -\Delta t \sum_{j=1}^N \nabla U_{\text{int}}(\mathbf{r}_i^{k,\alpha} - \mathbf{r}_j^{k,\alpha}) + \sqrt{2T(\mathbf{r}_i^{k,\alpha})} \Delta \boldsymbol{\eta}_i^k, \quad (18)$$

where the $\{\Delta \boldsymbol{\eta}_i^k\}$ are independent centered Gaussian random noises such that $\langle \Delta \eta_{i,\mu}^k \Delta \eta_{j,\nu}^\ell \rangle = \delta_{ij} \delta_{\mu\nu} \delta_{k\ell} \Delta t$. In Eq. (18),

$$\mathbf{r}_i^{k,\alpha} = \alpha \mathbf{r}_i^{k+1} + (1 - \alpha) \mathbf{r}_i^k = \mathbf{r}_i^k + \alpha \Delta \mathbf{r}_i^k. \quad (19)$$

Different values of α correspond to different physical processes. Note that, if one considers the large damping limit of the underdamped colloids studied in Sec. II, there is no ambiguity: As shown by Van Kampen [38], the overdamped limit then leads to the It \bar{o} discretization $\alpha = 0$. Other physical processes, that cannot be interpreted as Brownian colloids with position-dependent temperature, may lead to Eq. (17) with other discretizations [37]. For the sake of generality, we thus consider the case of a generic α discretization. For simplicity, we still refer to the amplitude of the multiplicative noise as a ‘temperature’, even when $\alpha \neq 0$.

These microscopic dynamics translate into an evolution equation for the fluctuating empirical density field $\hat{\rho}$, defined as:

$$\hat{\rho}(\mathbf{r}, t) \equiv \sum_i \delta(\mathbf{r} - \mathbf{r}_i(t)), \quad (20)$$

and for its average $\rho(\mathbf{r}) \equiv \langle \hat{\rho}(\mathbf{r}) \rangle$. For an α discretization, the evolution of ρ reads [49]

$$\dot{\rho}(\mathbf{r}, t) = \nabla \cdot \left[T(\mathbf{r})^\alpha \nabla \left\{ \rho(\mathbf{r}, t) T(\mathbf{r})^{1-\alpha} \right\} \right] \quad (21)$$

$$+ \int d^d \mathbf{r}' \langle \hat{\rho}(\mathbf{r}, t) \hat{\rho}(\mathbf{r}', t) \rangle \nabla U_{\text{int}}(\mathbf{r} - \mathbf{r}') \Big] \\ \equiv -\nabla \cdot \mathbf{J}(\mathbf{r}, t) \quad (22)$$

where we have introduced the particle current $\mathbf{J}(\mathbf{r}, t)$.

Below, we first review in Sec. III A the phenomenology of PBPs using numerical simulations. We then explore their TRS in Sec. III B. We first show that, for all α , non-interacting PBPs do not display steady currents due to an emergent TRS. We then calculate the non-zero entropy production induced by interactions between the particles. In Sec. III C, we show that effective momentum conservation forbids interaction-induced currents for the It \bar{o} -discretized system and the ‘Hänggi’ ($\alpha = 1$) time discretization, which is the time reverse of an It \bar{o} -discretized system. On the contrary, for $0 < \alpha < 1$, the multiplicative noise leads to net momentum sources and the emergence of ratchet currents. Finally, in Sec. III D, we characterize the onset of this ratchet current perturbatively in the interaction strength between particles.

A. Numerics and phenomenology

In the absence of interactions ($U_{\text{int}} = 0$), the steady-state density distribution satisfies

$$\rho_s(\mathbf{r}) \propto T(\mathbf{r})^{\alpha-1}, \quad (23)$$

as can be inferred from Eq. (21). The resulting current $\mathbf{J}(\mathbf{r})$ then vanishes, making this system an apparent exception to the ratchet principle.

Again, it is interesting that adding interactions induces a current for these systems *only* for discretizations $0 < \alpha < 1$, as demonstrated in Fig. 3. The $\alpha = 0$ (It \bar{o}) and $\alpha = 1$ (Hänggi) discretizations do not admit interaction-induced currents.

B. Time-reversal symmetry

We show below that noninteracting overdamped PBPs obey TRS regardless of their discretization. We prove this first by computing the path probabilities in Sec. III B 1 and then by demonstrating the symmetry of the Fokker-Planck operator in Sec. III B 2. We then turn to interacting particles in Sec. III B 3. In the rest of this article, we use either the path-probability or operator approach, depending on the context.

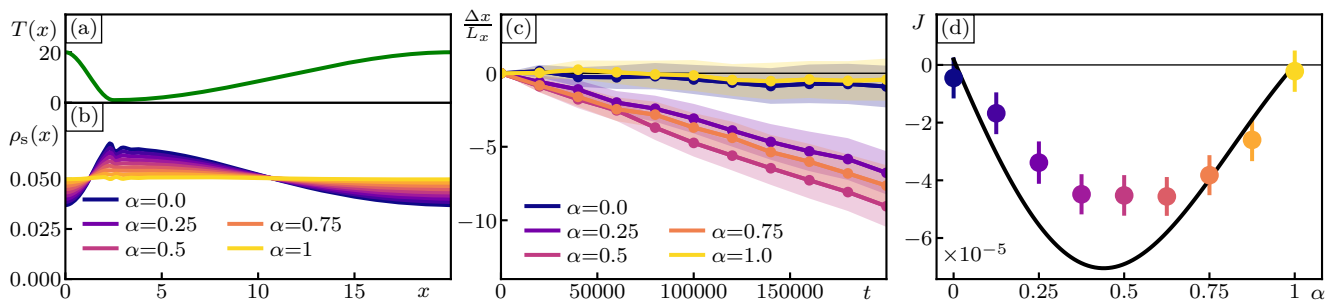


FIG. 3. **Interaction-induced current for PBPs with different time discretizations.** (a) Particles interacting via a soft repulsive harmonic potential, Eq. (A1), are placed in a temperature landscape $T(x)$. (b) Steady-state particle density as the time-discretization parameter α is varied. (c) The net integrated displacement of the particles show the emergence of nonzero currents for discretizations $0 < \alpha < 1$. (d) Steady-state particle current as α is varied. Momentum conservation prevents a ratchet current in the Itô-discretized ($\alpha=0$) system. The Hänggi-discretized ($\alpha=1$) system is equivalent to a time-reversed Itô dynamics and thus also current free. Finally, no such conservation exists in other discretizations which thus lead to ratchet currents. The mean-field prediction for the current J , to 1st-order in the interaction strength, Eq. (49), is plotted in black. Simulation details are provided in Appendix A 3.

1. TRS at the trajectory level

First, we set $U_{\text{int}} = 0$ to consider noninteracting particles. The system then reduces to a single-body problem and we omit below the particle index. When calculating the probabilities of trajectories, the multiplicative noise $T(\mathbf{r})$ calls for some care [49]. The corresponding time-discretized calculations are detailed in Appendix C 1, leading to a path probability for a trajectory $\mathbf{r}(t)$ starting at a given position $\mathbf{r}(0)$:

$$\begin{aligned} \mathbb{P}[\mathbf{r}(t)|\mathbf{r}(0)] &\propto F(\{\bar{\mathbf{r}}^k\}) \\ &\times \exp \left[\int_0^{t_f} dt \left\{ -\frac{|\dot{\mathbf{r}} - (\alpha - \frac{1}{2})\nabla T(\mathbf{r})|^2}{4T(\mathbf{r})} \right. \right. \\ &\left. \left. + \frac{(\alpha - \frac{1}{2})}{2} \left(\frac{|\nabla T(\mathbf{r})|^2}{2T(\mathbf{r})} - \nabla^2 T(\mathbf{r}) \right) - \frac{\dot{\mathbf{r}} \cdot \nabla T(\mathbf{r})}{4T(\mathbf{r})} \right\} \right], \end{aligned} \quad (24)$$

where F is a function of the discretized positions at the midpoint of each timestep, $\bar{\mathbf{r}}^k$, defined as

$$\bar{\mathbf{r}}^k = \frac{1}{2}\mathbf{r}^k + \frac{1}{2}\mathbf{r}^{k+1}. \quad (25)$$

While Eq. (24) describes the path-probability of Langevin dynamics for any values of α , the time-discretization used to construct *the path-integral* is the Stratonovich one, so that the standard chain rule can be used to compute integrals appearing in the exponent [49].

The probability of the reverse trajectory is found by replacing the trajectories with their time reverses,

$$\mathbf{r}(t) \mapsto \mathbf{r}^R(t) = \mathbf{r}(t_f - t), \quad (26)$$

$$\dot{\mathbf{r}}(t) \mapsto \dot{\mathbf{r}}^R(t) = -\dot{\mathbf{r}}(t_f - t). \quad (27)$$

Taking the ratio of the forward and reverse path probabilities results in the cancellation of all terms symmetric under time reversal, such as $|\dot{\mathbf{r}}|^2$, $F(\{\bar{\mathbf{r}}_k\})$, and all terms

that depend solely on \mathbf{r} . One then finds:

$$\begin{aligned} \frac{\mathbb{P}[\mathbf{r}(t)|\mathbf{r}(0)]}{\mathbb{P}[\mathbf{r}^R(t)|\mathbf{r}^R(0)]} &= \exp \left\{ \int_0^{t_f} dt (\alpha - 1) \frac{\dot{\mathbf{r}} \cdot \nabla T(\mathbf{r})}{T(\mathbf{r})} \right\} \\ &= \exp \left\{ (\alpha - 1) \ln \left[\frac{T(\mathbf{r}(t_f))}{T(\mathbf{r}(0))} \right] \right\} \\ &= \frac{T(\mathbf{r}(t_f))^{\alpha-1}}{T(\mathbf{r}(0))^{\alpha-1}} = \frac{\rho_s[\mathbf{r}(t_f)]}{\rho_s[\mathbf{r}(0)]}. \end{aligned} \quad (28)$$

One thus has that the probability of observing forward and backward trajectories are equal: $\mathbb{P}[\mathbf{r}(t)|\mathbf{r}(0)]\rho_s[\mathbf{r}(0)] = \mathbb{P}[\mathbf{r}^R(t)|\mathbf{r}^R(0)]\rho_s[\mathbf{r}^R(0)]$. Overdamped noninteracting PBPs with inhomogeneous temperature and arbitrary discretization are thus time-reversal symmetric, despite having a non-Boltzmann steady-state density. This explains why they do not lead to ratchet currents.

2. TRS at the operator level

Time reversal symmetry can also be read in the existence of a conjugation relation between the evolution operator and its adjoint [50–52]. While less physically transparent, the calculation is actually easier in the non-interacting case, and nicely complements the path integral approach presented above. It is also a gentle introduction to the active case, that will prove more involved. For a single PBP in a temperature field, the Fokker-Planck operator \mathcal{L}_{FP} , which satisfies $\partial_t \rho = -\mathcal{L}_{\text{FP}} \rho$, is given by $\mathcal{L}_{\text{FP}} = -\nabla \cdot T^\alpha \nabla T^{1-\alpha}$. Its adjoint is $\mathcal{L}_{\text{FP}}^\dagger = -T^{1-\alpha} \nabla \cdot T^\alpha \nabla$. Direct calculation then shows that:

$$\begin{aligned} \rho_s \mathcal{L}_{\text{FP}}^\dagger \rho_s^{-1} &= -\frac{C}{T^{1-\alpha}} T^{1-\alpha} \nabla \cdot T^\alpha \nabla \frac{T^{1-\alpha}}{C} \\ &= -\nabla \cdot T^\alpha \nabla T^{1-\alpha} = \mathcal{L}_{\text{FP}}, \end{aligned} \quad (29)$$

which implies detailed balance with respect to the non-Boltzmann steady-state distribution ρ_s .

3. Interaction-induced TRS violation

We now extend the path-integral calculation of Sec. III B 1 to the interacting case, $U_{\text{int}} \neq 0$, using again the general α discretization (18). This calculation is detailed in Appendix C 2 and leads to:

$$\begin{aligned} \mathbb{P}[\{\mathbf{r}_i(t)\}|\{\mathbf{r}_i(0)\}] &= K(\{\dot{\mathbf{r}}_i^k, |\Delta\mathbf{r}_i^k|^2\}) \\ &\times \exp \left[- \int_0^{t_f} dt \sum_{i=1}^N \left\{ \frac{\dot{\mathbf{r}}_i \cdot \nabla T(\mathbf{r}_i)}{4T(\mathbf{r}_i)} \right. \right. \\ &\quad \left. \left. - \frac{\dot{\mathbf{r}}_i \cdot \left[(\alpha - \frac{1}{2}) \nabla T(\mathbf{r}_i) + \sum_j \mathbf{f}_{\text{int}}(\mathbf{r}_i - \mathbf{r}_j) \right]}{2T(\mathbf{r}_i)} \right\} \right]. \end{aligned} \quad (30)$$

Again, we can use this expression to evaluate the probability to observe the reverse trajectory $\mathbf{r}_i^R(t) = \mathbf{r}_i(t_f - t)$. Taking care of the discretization issues, we obtain the probability of the reverse trajectory, from which we calculate the entropy production as

$$\begin{aligned} \Sigma &\equiv \ln \left[\frac{\mathbb{P}[\{\mathbf{r}_i(t)\}|\{\mathbf{r}_i(0)\}]}{\mathbb{P}[\{\mathbf{r}_i^R(t)\}|\{\mathbf{r}_i^R(0)\}]} \right] \\ &= - \int_0^{t_f} dt \sum_{i=1}^N \frac{\dot{\mathbf{r}}_i \cdot [(\alpha - 1) \nabla T(\mathbf{r}_i) - \sum_j \mathbf{f}_{\text{int}}(\mathbf{r}_i - \mathbf{r}_j)]}{T(\mathbf{r}_i)} \\ &= \sum_{i=1}^N \ln \left[\frac{T(\mathbf{r}_i(t_f))^{\alpha-1}}{T(\mathbf{r}_i(0))^{\alpha-1}} \right] + \int_0^{t_f} dt \sum_{i,j=1}^N \frac{\dot{\mathbf{r}}_i \cdot \mathbf{f}_{\text{int}}(\mathbf{r}_i - \mathbf{r}_j)}{T(\mathbf{r}_i)}. \end{aligned} \quad (31)$$

The boundary terms in Eq. (31) do not contribute to the EPR and we find:

$$\sigma = \lim_{t_f \rightarrow \infty} \frac{1}{t_f} \Sigma = \int d\mathbf{r} \langle \hat{\sigma}(\mathbf{r}) \rangle, \quad (32)$$

where in the last step we have invoked ergodicity and introduced an entropy density

$$\hat{\sigma}(\mathbf{r}) = - \sum_{i,j} \delta(\mathbf{r} - \mathbf{r}_i) \frac{\dot{\mathbf{r}}_i \cdot \nabla U_{\text{int}}(\mathbf{r}_i - \mathbf{r}_j)}{T(\mathbf{r}_i)}. \quad (33)$$

This can be rewritten in a thermodynamically inspired form as

$$\hat{\sigma}(\mathbf{r}, t) = \sum_i \delta(\mathbf{r} - \mathbf{r}_i) \frac{\dot{Q}_i}{T(\mathbf{r}_i)}, \quad (34)$$

where $\dot{Q}_i \equiv - \sum_j \dot{\mathbf{r}}_i \cdot \nabla U_{\text{int}}(\mathbf{r}_i - \mathbf{r}_j)$ can be interpreted as the heat dissipation rate of the i th particle. Interestingly, this expression is independent of the discretization α and shows that σ is generically non-zero. The irreversibility of the dynamics is confirmed using particle-based simulations with an Itô discretization ($\alpha = 0$) in Fig. 4.

C. Effective momentum conservation

In this section, we show that, despite having a finite EPR, PBPs with Itô discretization do not exhibit ratchet

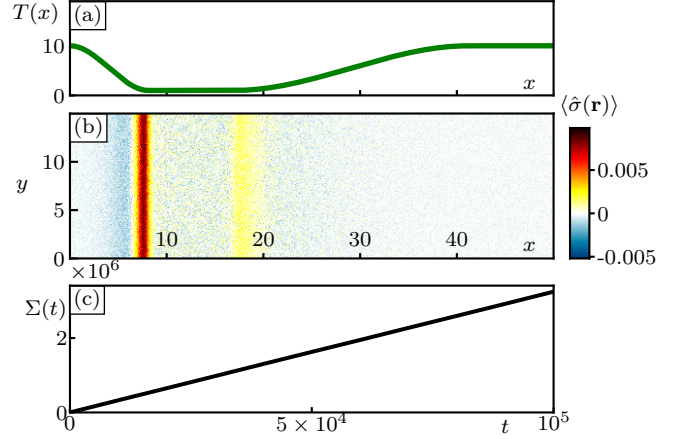


FIG. 4. **EPR measured in simulations of overdamped PBPs.** (a) Temperature landscape. (b) Heat map of the average EPR density field $\langle \hat{\sigma}(\mathbf{r}) \rangle$. (c) Net entropy production up to time t . Adapted from Fig. 2 of our companion letter [44]. Simulation details are provided in Appendix A 3.

currents. As for U-PBPs, this can be explained by an emergent bulk momentum conservation which prevents the existence of the momentum sources required to rectify fluctuations into motion. We first rewrite Eq. (21) as

$$\begin{aligned} \dot{\rho} &= \nabla \cdot \left\{ \nabla(T\rho) - \int d^d \mathbf{r}' \langle \hat{\rho}(\mathbf{r}) \hat{\rho}(\mathbf{r}') \rangle \mathbf{f}_{\text{int}}(\mathbf{r} - \mathbf{r}') - \alpha \rho \nabla T \right\} \\ &\equiv \nabla \cdot \{ \nabla \cdot [\mathbb{I} \rho T - \boldsymbol{\sigma}_{\text{IK}}] - \alpha \rho \nabla T \} \\ &\equiv - \nabla \cdot \{ \nabla \cdot \boldsymbol{\sigma}_{\text{tot}} + \delta \mathbf{F}_{\text{P}}^{(\alpha)} \}, \end{aligned} \quad (35)$$

where we have again introduced the Irving-Kirkwood stress tensor defined in Eq. (15). The term that could not be written as the divergence of a stress tensor leads to the nonconservative force $\delta \mathbf{F}_{\text{P}}^{(\alpha)} \equiv \alpha \rho \nabla T$. Thus we can write the current as the sum of momentum-conserving and nonconserving parts as

$$\mathbf{J} = \nabla \cdot \boldsymbol{\sigma}_{\text{tot}} + \delta \mathbf{F}_{\text{P}}^{(\alpha)}. \quad (36)$$

This has important, discretization-dependent consequences for the presence of steady-state ratchet currents.

First, let us consider the case of Itô discretization $\alpha = 0$. In this case, the nonconservative force vanishes $\delta \mathbf{F}_{\text{P}}^{(\alpha)} = 0$, and the current can be written as the divergence of a stress tensor, as for U-PBPs (Sec. II C). Thus by the same reasoning, the current vanishes everywhere.

When $\alpha \neq 0$, however, $\delta \mathbf{F}_{\text{P}}^{(\alpha)}$ may act as a momentum source in regions with temperature gradients. Thus there is no apparent symmetry preventing the emergence of ratchet currents.

D. Emergence of interaction-induced current

In this section, we demonstrate that a current arises for $0 < \alpha < 1$ using a factorization approximation. To make progress, we focus on systems with translational symmetry in all but one directions, using $T(\mathbf{r}) = T(x)$. Further, to close Eq. (35), we factorize the pair-correlation function as

$$\langle \hat{\rho}(x)\hat{\rho}(x') \rangle \approx \langle \hat{\rho}(x) \rangle \langle \hat{\rho}(x') \rangle = \rho(x)\rho(x'). \quad (37)$$

This approximation becomes accurate when correlations between particles can be neglected, e.g. in the weak interaction, large density, or high-dimensional limits. These simplifications allow us to rewrite Eq. (21) as

$$\begin{aligned} \dot{\rho} &= \partial_x \left[T^\alpha \partial_x (\rho T^{1-\alpha}) + \rho(x) \int dx' \rho(x') U'_{\text{int}}(x-x') \right] \\ &= \partial_x \left[\partial_x (\rho T) - \alpha \rho \partial_x T + \rho \partial_x V_{\text{eff}} \right] \\ &= \partial_x \left[\partial_x (\rho T) - \rho F_{\text{eff}}(x) \right], \end{aligned} \quad (38)$$

where we have defined an effective potential V_{eff} and effective total force F_{eff} as:

$$V_{\text{eff}}(x) \equiv (U_{\text{int}} * \rho)(x) = \int dx' \rho(x') U_{\text{int}}(x-x'), \quad (39)$$

$$F_{\text{eff}}(x) \equiv \alpha T'(x) - \partial_x V_{\text{eff}}(x). \quad (40)$$

Equations (38)-(40) show that the factorization approximation maps the system onto the dynamics of an α -discretized single particle that experiences a mean-field effective potential V_{eff} created by the other particles, or equivalently of an Itô-discretized particle that experiences an effective force field F_{eff} .

Before solving this nonlinear equation perturbatively (and self-consistently) in the interaction strength, we first review the simpler, non-interacting problem where $F_{\text{eff}}(x)$ is an arbitrary *external* force, which was solved by van Kampen [38]. In addition to its pedagogical purpose, this allows us to fix a typo in [38] and introduce useful notations.

1. A single particle in potential, temperature, and mobility fields

Van Kampen considered a single PBP in a temperature field $T_{\text{eff}}(x)$, mobility field $\mu_{\text{eff}}(x)$, and external force field $F_{\text{eff}}(x)$, described by the Fokker-Planck equation

$$\dot{\rho} = \partial_x \left\{ \mu_{\text{eff}} \left[\partial_x (T_{\text{eff}} \rho) - \rho F_{\text{eff}} \right] \right\} \equiv -\partial_x J. \quad (41)$$

Direct algebra shows that the steady-state solution is given by [38]

$$\begin{aligned} \rho(x) &= \frac{e^{-\Phi(x)}}{T_{\text{eff}}(x)} \left[\rho(0) T_{\text{eff}}(0) - J \int_0^x du \frac{e^{\Phi(u)}}{\mu_{\text{eff}}(u)} \right], \quad (42) \\ J &= \frac{e^{-\Phi(L)} - 1}{\int_0^L \frac{dx e^{-\Phi(x)}}{T_{\text{eff}}(x)} \left[\int_0^x \frac{dx' e^{\Phi(x')}}{\mu_{\text{eff}}(x')} + \int_x^L \frac{dx' e^{\Phi(x') - \Phi(L)}}{\mu_{\text{eff}}(x')} \right]}, \end{aligned} \quad (43)$$

where $\rho(0)$ is a constant such that ρ is normalized [38] and the ‘‘pseudo-potential’’ Φ is given by

$$\Phi(x) \equiv - \int_0^x \frac{F_{\text{eff}}(x')}{T_{\text{eff}}(x')} dx'. \quad (44)$$

We note that $T_{\text{eff}}(0)$ in Eq. (42) was mistakenly written as $T_{\text{eff}}(x)$ in [38].

One sees that a nonzero current arises if and only if $\Phi(L) \neq 0$; i.e., when Φ is aperiodic:

$$J \neq 0 \iff \Phi(L) \neq 0. \quad (45)$$

Let us now show how we can use the non-interacting solution given in Eqs. (42)-(44) to solve the interacting problem perturbatively.

2. Perturbation theory

To perform a perturbative expansion in the interaction strength, we introduce a rescaled potential \tilde{U}_{int} such that $U_{\text{int}} = \varepsilon \tilde{U}_{\text{int}}$ and we use ε as a small parameter. We then use the solution (42)-(44) to Eq. (38) with $T_{\text{eff}} = T(x)$, $\mu_{\text{eff}} = 1$, and $F_{\text{eff}} = \alpha T' - \varepsilon (\tilde{U}_{\text{int}} * \rho)'$ to show that the steady-state density satisfies the self-consistent integral equation:

$$\begin{aligned} \rho &= \frac{\exp \left(-\varepsilon \int_0^x du \frac{(\tilde{U}_{\text{int}} * \rho)'}{T} \right)}{T^{1-\alpha}} \\ &\times \left[\kappa - J \int_0^x du \frac{\exp \left(\varepsilon \int_0^u du' \frac{(\tilde{U}_{\text{int}} * \rho)'}{T} \right)}{T^\alpha} \right] \end{aligned} \quad (46)$$

where $\kappa \equiv \rho(0)T(0)^{1-\alpha}$ is a normalization constant such that $\int dx \rho(x) = N$. Next, we insert the expansion

$$\rho(x) = \sum_{k=0}^{\infty} \varepsilon^k \rho_k(x), \quad J = \sum_{k=0}^{\infty} \varepsilon^k J_k \quad (47)$$

into Eq. (46), which we solve order by order. At zeroth order, we recover the solution Eq. (23) which describes noninteracting particles: $\rho_0 = \kappa_0/T^{1-\alpha}$ and $J_0 = 0$, where $\kappa_0 = N \left[\int_0^L T(u)^{\alpha-1} \right]^{-1}$. Then, the first order

correction to the density field and current are given by

$$\rho_1 = \frac{1}{T^{1-\alpha}} \left\{ \kappa_1 - \int_0^x du \left[\kappa_0 \frac{(\tilde{U}_{\text{int}} * \rho_0)'(u)}{T(u)} + \frac{J_1}{T(u)^\alpha} \right] \right\}. \quad (48)$$

$$J_1 = -\frac{\kappa_0^2}{\int_0^L \frac{dx}{T(x)^\alpha}} \int_0^L dx \int_0^L dx' \frac{\tilde{U}'_{\text{int}}(x-x')}{T(x)T(x')^{1-\alpha}}, \quad (49)$$

where κ_1 is such that $\int_0^L \rho_1(x)dx = 0$ and J_1 enforces the periodicity of ρ_1 . We thus see that a non-vanishing current emerges at first order in the interaction amplitude. Already, this result captures semi-quantitatively the trend shown in numerical simulations of interacting particles, as seen in Fig. 3d. The perturbation expansion can then be solved systematically to higher order, in the spirit of what will be done below for one-dimensional RTPs in Sec. IV D 2.

Consistent with Sec. III C, J_1 vanishes for the It \bar{o} -discretization $\alpha = 0$, since $\tilde{U}'_{\text{int}}(x-x')$ is antisymmetric under $x \leftrightarrow x'$, while the denominator in Eq. (49) is symmetric for $\alpha = 0$. Interestingly, J_1 also vanishes for $\alpha = 1$, since $J_1 \propto [\tilde{U}_{\text{int}}(x+L) - \tilde{U}_{\text{int}}(x)] = 0$ in this case. For other values of α , however, J_1 is generally nonzero if T is asymmetric, consistent with the numerical results shown in Fig. 3d.

Note that one can show the current to vanish exactly for the $\alpha = 1$ Hänggi discretization. Although it appears to lack momentum conservation according to Eq. (35), a Hänggi-discretized trajectory is equivalent to the time-reverse of an It \bar{o} -discretized one, with a force of the opposite sign. In fact, one can perform the same mapping between any α -discretized trajectory and a $(1-\alpha)$ -discretized one, since Eq. (18) can be re-written as

$$-\Delta \mathbf{r}_i^{R,k} = -\sum_j \nabla U_{\text{int}}(\mathbf{r}_i^{R,k+1} - \mathbf{r}_j^{R,k+1}) \Delta t + \sqrt{2T(\mathbf{r}_i^{R,k} + (1-\alpha)\Delta \mathbf{r}_i^{R,k+1})} \Delta \boldsymbol{\eta}_i^{R,k+1} \quad (50)$$

where the reverse trajectory is defined as $\mathbf{r}_i^{R,k} \equiv \mathbf{r}_i^{N-k}$. Setting $\alpha = 0$, we find that the trajectory \mathbf{r}_i^R is identical to a Hänggi-discretized overdamped PBP with interaction potential $-U_{\text{int}}$. Since the current of an It \bar{o} -discretized trajectory must be zero regardless of the sign of its force due to the effective momentum conservation, the time-reverse of any It \bar{o} -discretized trajectory must also have zero current. Therefore, the interaction-induced ratchet current vanishes for both $\alpha = 0$ and $\alpha = 1$.

E. Summary

Overdamped PBPs with inhomogeneous temperature, perhaps the first recognized “exception” to the ratchet principle [37, 38], display a surprisingly rich phenomenology when interactions and various choices of time discretizations are considered.

We have seen that spatially varying temperature fields cannot alone power steady-state currents, regardless of discretization scheme, due to the TRS of the dynamics. This TRS is broken when interparticle interactions are introduced, as reflected in the EPR shown in Eq. (33), which does not depend on the discretization. Despite this TRS violation, It \bar{o} -discretized PBPs obey a bulk momentum conservation which prevents them from exhibiting a current. Furthermore, Hänggi-discretized PBPs are equivalent to the time-reverse of It \bar{o} -discretized PBPs with an opposite force, and thus also exhibit no ratchet current.

On the contrary, for discretizations $0 < \alpha < 1$ —and notably for the Stratonovich discretization $\alpha = 1/2$ —there are momentum sources, as shown in Eq. (35), which power steady-state ratchet currents. We have measured these currents in particle-based simulations (Fig. 3) and analytically approximated them in Eq. (49) using a factorization approximation and a perturbative expansion.

IV. ACTIVE-BROWNIAN AND RUN-AND-TUMBLE PARTICLES

Next, we move our focus to Active Brownian Particles (ABPs) and Run-and-Tumble Particles (RTPs) with spatially varying activity. We consider these two systems together because, as we will demonstrate, their behaviors are quite similar to each other. Again, we introduce the models, briefly discuss their phenomenologies, and examine time-reversal symmetry and momentum conservation. Finally, we discuss the characterization of the emergence of interaction-induced currents using a perturbation theory.

We consider N self-propelled particles in d dimensions with the spatial dynamics

$$\dot{\mathbf{r}}_i = v(\mathbf{r}_i) \mathbf{u}_i(t) - \sum_j \nabla U_{\text{int}}(\mathbf{r}_i - \mathbf{r}_j), \quad (51)$$

where $\mathbf{r}_i \in \mathbb{R}^d$ is the position of particle i , $\mathbf{u}_i \in \mathcal{S}^{d-1}$ is its orientation director on the $(d-1)$ -sphere, and U_{int} is the pairwise interaction potential. For ABPs, the director undergoes rotational diffusion on the $(d-1)$ -sphere, with diffusivity D_r . In $d = 2$, which is the case where most of our computations will be done, $\mathbf{u}_i(\theta_i) = (\cos \theta_i, \sin \theta_i)$ and the dynamics reads

$$\dot{\theta}_i = \sqrt{2D_r} \eta_i, \quad (52)$$

where η_i is a Gaussian white noise such that

$$\langle \eta_i(t) \eta_j(t') \rangle = \delta_{ij} \delta(t-t'). \quad (53)$$

For RTPs, the orientation director undergoes a complete randomization with a rate α :

$$\mathbf{u}_i \xrightarrow{\alpha} \mathbf{u}'_i \quad (54)$$

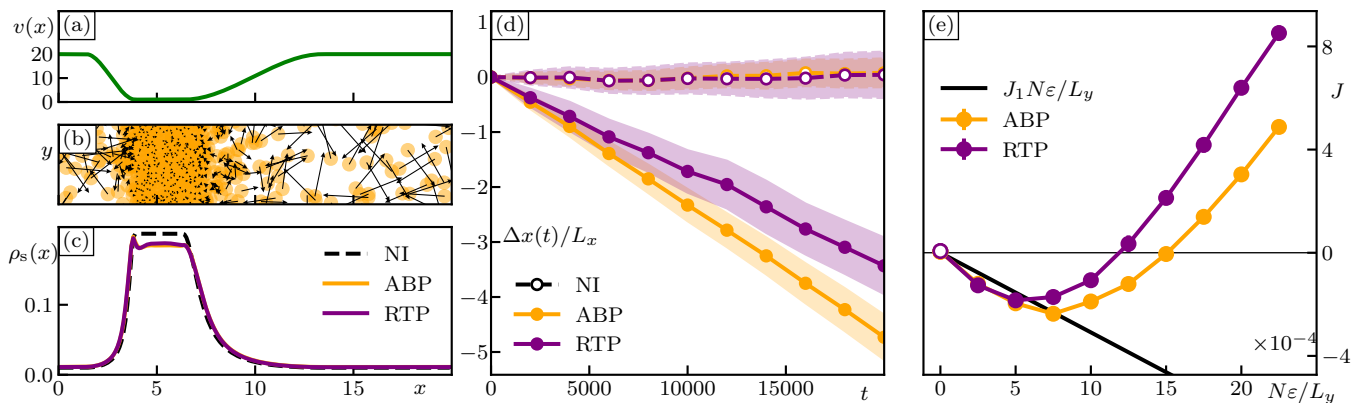


FIG. 5. **Interaction-induced current for ABPs and RTPs in $d = 2$ spatial dimensions.** We use a soft repulsive harmonic potential proportional to ε . (a) Self-propulsion landscape $v(x)$ used in all simulations. Panels (b-d) correspond to simulations with $N\varepsilon/L_y = 7.5$. (b) Snapshot of particle locations and self-propulsion vectors for an ABP simulation. (c) Steady-state density distributions, compared to the non-interacting result $\rho_s(x) \propto 1/v(x)$. (d) Net average displacement per particle over time for interacting (solid) and non-interacting (dashed) ABPs and RTPs. The shaded region indicates $\pm 3\sigma$, where σ is the standard error of the mean. (e) Average current vs. interaction strength, along with the mean-field prediction to first order in ε . Simulation details are provided in Appendix A 4.

where \mathbf{u}'_i is sampled from a uniform distribution on S^{d-1} . For RTPs in 1d, \mathbf{u}_i is restricted to $\{+1, -1\}$. We denote the persistence times by $\tau = 1/\alpha$ for RTPs and $\tau = 1/[(d-1)D_r]$ for ABPs.

We define the empirical density in (\mathbf{r}, \mathbf{u}) space as $\hat{\psi}(\mathbf{r}, \mathbf{u}) = \sum_i \delta(\mathbf{r} - \mathbf{r}_i) \delta(\mathbf{u} - \mathbf{u}_i)$, along with its average over noise realizations, $\psi(\mathbf{r}, \mathbf{u}) = \langle \hat{\psi}(\mathbf{r}, \mathbf{u}) \rangle$. Standard methods [40, 45] allow us to convert (51)-(54) into:

$$\begin{aligned} \dot{\psi}(\mathbf{r}, \mathbf{u}, t) = & \mathcal{L}_r \psi(\mathbf{r}, \mathbf{u}) - \nabla \cdot \left[v(\mathbf{r}) \mathbf{u} \psi(\mathbf{r}, \mathbf{u}) \right. \\ & \left. - \int d^d \mathbf{r}' \int d^{d-1} \mathbf{u}' \nabla U_{\text{int}}(\mathbf{r} - \mathbf{r}') \langle \hat{\psi}(\mathbf{r}, \mathbf{u}) \hat{\psi}(\mathbf{r}', \mathbf{u}') \rangle \right]. \end{aligned} \quad (55)$$

We have defined an operator \mathcal{L}_r which accounts for the dynamics of the orientation \mathbf{u} . For RTPs, it reads

$$\mathcal{L}_r \psi = -\alpha \psi(\mathbf{r}, \mathbf{u}) + \frac{\alpha}{\Omega_d} \int d^{d-1} \mathbf{u}' \psi(\mathbf{r}, \mathbf{u}') \quad (56)$$

while for ABPs it is given by

$$\mathcal{L}_r \psi = D_r \Delta_{\mathbf{u}} \psi, \quad (57)$$

where $\Delta_{\mathbf{u}}$ is the Laplacian on the $(d-1)$ -dimensional sphere.

In the following sections, we show through a combination of exact calculations, motivated approximations, and particle-based simulations that non-interacting ABPs and RTPs in d dimensions are prevented from exhibiting ratchet currents by a hidden time-reversal symmetry (TRS), which is destroyed in the presence of interactions. The lack of momentum conservation then generically induces a ratchet current, which we calculate perturbatively using a factorization approximation.

A. Numerics and phenomenology

ABPs have been shown numerically to experience interaction-induced current in [42]. In Fig. 5, we characterize quantitatively the emergence of ratchet currents for ABPs and RTPs in $d = 2$ spatial dimensions. Non-interacting ABPs and RTPs in an activity landscape $v(\mathbf{r})$ relax to an isotropic, current-free steady state with $\psi_s(\mathbf{r}, \mathbf{u}) \propto 1/v(\mathbf{r})$ [39, 53–55], as can be inferred from Eq. (55). Introducing interactions perturbs the density distribution and destroys the current-free state [Fig. 5(d)]. The resulting current can be very strong and sometimes exhibits reversals [Fig. 5(e)].

B. Time-reversal symmetry

In this section we show that, in the absence of interactions, ABPs and RTPs in varying activity landscape satisfy TRS in position space. While computing the EPR in the full (\mathbf{r}, \mathbf{u}) space indeed leads to a positive number [56–59], we show below that this apparent irreversibility disappears when only tracking the particle positions.

As for PBPs, we first show this at the level of trajectory. The algebra is much more involved and we do it only for RTP in $d = 1$ before treating the general case at the operator level.

1. TRS at the trajectory level for 1d RTPs

Let us start by considering the dynamics of an RTP in one space dimension, whose dynamics reads

$$\dot{x} = v(x)u(t), \quad (58)$$

$$u \xrightarrow{\alpha} u' \in \{-1, 1\}. \quad (59)$$

We note that the particle position evolves deterministically between tumbles and use this below to prove time-reversal symmetry in position space.

We consider a trajectory $\{x(t), u(t)\}$ in a time interval $t \in [t_i, t_f]$, with the boundary conditions $x(t_{i,f}) = x_{i,f}$ and $u(t_{i,f}) = u_{i,f}$. Without loss of generality, we simplify our notations by setting $t_i = 0$ and $t_f = \tau$. If the time evolution of the orientation $\{u(t)\}$ is specified, the probability density for the position evolves according to

$$\partial_t P(x, t | \{u(t)\}, x_i) = -\partial_x [v(x)u(t)P]. \quad (60)$$

The solution to Eq. (60) is

$$P(x, t | \{u(t)\}, x_i) = \delta[x - X(t|x_i)], \quad (61)$$

where $X(t|x_i)$ is the solution to $\dot{X}(t) = v(X)u(t)$ with $X(0) = x_i$, which can be verified directly by plugging Eq. (61) into Eq. (60).

Next, we consider the time-reversed evolution of the particle in position space, that is realized by reversing its orientation:

$$x(t) \mapsto x^R(t) = x(\tau - t), \quad (62)$$

$$u(t) \mapsto u^R(t) = -u(\tau - t). \quad (63)$$

Similar to Eq. (61), the probability density conditioned on the reversed orientation satisfies

$$P(x, t | \{u^R(t)\}, x_f) = \delta[x - X^R(t|x_f)] \quad (64)$$

where $X^R(t|x_f)$ is the solution of $\dot{X}^R(t) = v(X^R)u^R(t)$ with the initial position $X^R(0) = x_f$.

Equation (61) implies that

$$P(x_f, \tau | \{u(t)\}, x_i) = \delta[g_f(x_f, x_i)], \quad (65)$$

with $g_f(x_f, x_i) = x_f - X(\tau|x_i)$. Similarly, introducing $g_i(x_f, x_i) = x_i - X^R(\tau|x_f)$, Eq. (64) implies that

$$P(x_i, \tau | \{-u(t)\}, x_f) = \delta[g_i(x_f, x_i)]. \quad (66)$$

We note that g_f and g_i vanish on the same one-dimensional subset of \mathbb{R}^2 that we denote by \mathcal{C} . Let us now show that

$$\frac{P(x_i, \tau | \{u^R(t)\}, x_f)}{P(x_f, \tau | \{u(t)\}, x_i)} = \frac{v(x_f)}{v(x_i)}. \quad (67)$$

Consider a function $f(\mathbf{x}) \equiv f(x_i, x_f)$, then

$$\int_{\mathbb{R}^2} f(\mathbf{x}) \delta[g_f(\mathbf{x})] d\mathbf{x} = \int_{\mathcal{C}} \frac{f(\mathbf{x}) d\sigma(\mathbf{x})}{|\nabla g_f|} \quad (68)$$

where $d\sigma(\mathbf{x})$ is the Minkowsky content measure of \mathcal{C} and $\nabla = (\partial_{x_f}, \partial_{x_i})$. In turn, Eq. (68) can be written as

$$\int_{\mathcal{C}} \frac{|\nabla g_i|}{|\nabla g_f|} \frac{f(\mathbf{x}) d\sigma(\mathbf{x})}{|\nabla g_i|} = \int_{\mathbb{R}^2} f(\mathbf{x}) \frac{|\nabla g_i|}{|\nabla g_f|} \delta[g_i(\mathbf{x})] d\mathbf{x} \quad (69)$$

Identifying Eqs. (68) and (69) then leads to $\delta[g_f(\mathbf{x})] = \delta[g_i(\mathbf{x})] |\nabla g_i| / |\nabla g_f|$. Computing the gradients explicitly, we find

$$\frac{P(x_i, \tau | \{u^R(t)\}, x_f)}{P(x_f, \tau | \{u(t)\}, x_i)} = \frac{\sqrt{1 + (dX(\tau|x_i)/dx_i)^2}}{\sqrt{1 + (dX^R(\tau|x_f)/dx_f)^2}}. \quad (70)$$

To proceed, we rewrite $dX(t)/dt = v(X)u(t)$ as $dt = dX(t)/[v(X)u(t)]$, which we integrate to get

$$\tau = \int_{x_i}^{X(\tau)} \frac{dx}{v(x)u[t(x)]}. \quad (71)$$

Differentiating Eq. (71) with respect to x_i and rearranging leads to

$$\left| \frac{dX(\tau|x_i)}{dx_i} \right| = \frac{v(x_f)}{v(x_i)}. \quad (72)$$

Similarly, for the time-reversed realization, we obtain

$$\left| \frac{dX^R(\tau|x_f)}{dx_f} \right| = \frac{v(x_i)}{v(x_f)}. \quad (73)$$

Plugging Eqs. (72) and (73) into Eq. (70), we obtain Eq. (67).

Since $\{u(t)\}$ follows a Poisson process with rate α and the tumbles randomly sample new orientations isotropically, the probability density for the time-reversed realization satisfies $\mathbb{P}[\{u^R(t)\}] = \mathbb{P}[\{u(t)\}]$. The propagator from x_i, u_i to x_f, u_f is then found by summing over the realizations of the orientation trajectory:

$$\begin{aligned} & P(x_f, u_f, \tau | x_i, u_i, 0) \\ &= \int \mathcal{D}[u(t)] \mathbb{P}[\{u(t)\}] P(x_f, \tau | \{u(t)\}, x_i) \\ &= \int \mathcal{D}[u(t)] \mathbb{P}[\{u^R(t)\}] P(x_i, \tau | \{u^R(t)\}, x_f) \frac{v(x_i)}{v(x_f)}, \end{aligned}$$

where we have used Eq. (70) in the last line and the path-integral over u is constrained to $u(0) = u_i$ and $u(\tau) = u_f$. Since $u^R(t) \rightarrow u(t)$ is an involution, there is no Jacobian in the corresponding change of variables, and we find

$$P(x_f, u_f, \tau | x_i, u_i, 0) = P(x_i, -u_i, \tau | x_f, -u_f, 0) \frac{v(x_i)}{v(x_f)}. \quad (74)$$

Let us now show that this implies TRS in position space. Considering that the system is in the steady state at time 0, the probability to be in x_i at time 0 and in x_f at time τ is given by

$$\begin{aligned} P(x_f, \tau; x_i, 0) &= \sum_{u_f, u_i} P(x_f, u_f, \tau; x_i, u_i, 0) \\ &= \sum_{u_f, u_i} P(x_f, u_f, \tau | x_i, u_i, 0) \psi_s(x_i, u_i), \end{aligned} \quad (75)$$

where we have used the definition of a conditional probability and ψ_s is the steady state measure. Using Eq. (74), one then find

$$P(x_f, \tau; x_i, 0) = \sum_{u_f, u_i} P(x_i, -u_i, \tau | x_f, -u_f, 0) \psi_s(x_i, u_i) \frac{v(x_i)}{v(x_f)}.$$

Using that $\psi_s(x, u) \propto 1/v(x)$, we then find

$$\begin{aligned} P(x_f, \tau; x_i, 0) &= \sum_{u_f, u_i} P(x_i, -u_i, \tau | x_f, -u_f, 0) \psi_s(x_f, -u_f) \\ &= P(x_i, \tau; x_f, 0). \end{aligned} \quad (76)$$

The dynamics is thus time-reversal symmetric in position space.

2. RTPs and ABPs in d dimensions

Let us now show the existence of TRS in position space using an operator approach for RTPs and ABPs in d dimensions. Consider Eqs. (51) and (55) in the absence of interactions. The corresponding Master equation can be written as

$$\dot{\psi}(\mathbf{r}, \mathbf{u}, t) = -\nabla \cdot [v(\mathbf{r})\mathbf{u}\psi] + \mathcal{L}_r \psi \equiv \mathcal{L}\psi \quad (77)$$

where we have introduced the evolution operator

$$\mathcal{L} = -\nabla \cdot v(\mathbf{r})\mathbf{u} + \mathcal{L}_r(\mathbf{u}), \quad (78)$$

and \mathcal{L}_r is the Hermitian evolution operator of the angular dynamics. The adjoint evolution operator reads $\mathcal{L}^\dagger = v(\mathbf{r})\mathbf{u} \cdot \nabla + \mathcal{L}_r(\mathbf{u})$. We remind that, in the non-interacting case, the steady-state solution satisfies $\psi_s(\mathbf{r}, \mathbf{u}) = \psi_s(\mathbf{r}, -\mathbf{u}) = \kappa/v(\mathbf{r})$, where κ is determined by normalization.

Direct algebra shows that

$$\mathcal{L}^\dagger = \psi_s^{-1} \Pi^{-1} \mathcal{L} \Pi \psi_s, \quad (79)$$

where the operator Π is such that with $\Pi f(\mathbf{r}, \mathbf{u}) = f(\mathbf{r}, -\mathbf{u})$. Let us now show that Eq. (79) implies TRS in position space. We consider that the system is in the steady state at time 0 and compute $P(\mathbf{r}', t, \mathbf{r}, 0)$, the probability to be at \mathbf{r} at time 0 and \mathbf{r}' at time t . Using Dirac bra-ket notations for the propagator, we find

$$\begin{aligned} P(\mathbf{r}', t, \mathbf{r}, 0) &= \int d\mathbf{u} d\mathbf{u}' P(\mathbf{r}', \mathbf{u}', t, \mathbf{r}, \mathbf{u}, 0) \\ &= \int d\mathbf{u} d\mathbf{u}' \langle \mathbf{r}', \mathbf{u}' | e^{t\mathcal{L}} | \mathbf{r}, \mathbf{u} \rangle \psi_s(\mathbf{r}, \mathbf{u}) \\ &= \int d\mathbf{u} d\mathbf{u}' \langle \mathbf{r}, \mathbf{u} | e^{t\mathcal{L}^\dagger} | \mathbf{r}', \mathbf{u}' \rangle \psi_s(\mathbf{r}, \mathbf{u}), \end{aligned} \quad (80)$$

where, in the last equality, we have used that the propagator $\langle \mathbf{r}', \mathbf{u}' | e^{t\mathcal{L}} | \mathbf{r}, \mathbf{u} \rangle$ is a real number and hence equal

to its adjoint. Equation (79) then tells us that

$$\begin{aligned} \langle \mathbf{r}, \mathbf{u} | e^{t\mathcal{L}^\dagger} | \mathbf{r}', \mathbf{u}' \rangle &= \langle \mathbf{r}, \mathbf{u} | \psi_s^{-1} \Pi^{-1} e^{t\mathcal{L}} \Pi \psi_s | \mathbf{r}', \mathbf{u}' \rangle \\ &= \frac{\psi_s(\mathbf{r}', \mathbf{u}')}{\psi_s^*(\mathbf{r}, \mathbf{u})} \langle \mathbf{r}, \mathbf{u} | \Pi^{-1} e^{t\mathcal{L}} \Pi | \mathbf{r}', \mathbf{u}' \rangle \\ &= \frac{\psi_s(\mathbf{r}', \mathbf{u}')}{\psi_s(\mathbf{r}, \mathbf{u})} \langle \mathbf{r}, -\mathbf{u} | e^{t\mathcal{L}} | \mathbf{r}', -\mathbf{u}' \rangle. \end{aligned} \quad (81)$$

Equations (80) and (81) then lead to

$$\begin{aligned} P(\mathbf{r}', t, \mathbf{r}, 0) &= \int d\mathbf{u} d\mathbf{u}' \psi_s(\mathbf{r}', \mathbf{u}') P(\mathbf{r}, -\mathbf{u}, t | \mathbf{r}', -\mathbf{u}', 0) \\ &= P(\mathbf{r}, t, \mathbf{r}', 0), \end{aligned} \quad (82)$$

where we have used that $\psi_s(\mathbf{r}', \mathbf{u}') = \psi_s(\mathbf{r}', -\mathbf{u}')$ in the final line.

Thus, ABPs and RTPs with spatially varying self-propulsion obey TRS in position space and cannot experience ratchet currents.

3. Interaction-induced TRS violations

Interacting active matter has frequently been shown to exhibit nonzero entropy production in position space [26, 27, 60–62]. In fact, for ABPs and RTPs without translational diffusivity, pairwise forces typically make the dynamics fully irreversible. This can be made apparent by considering the interacting dynamics Eq. (51):

$$\dot{\mathbf{r}}_i(t) = \mathbf{F}_i(\{\mathbf{r}_j(t)\}) + v(\mathbf{r}_i(t))\mathbf{u}_i(t). \quad (83)$$

We note that, for the time-reversed realization of \mathbf{r} to be solution of the dynamics, it also needs to satisfy

$$\dot{\mathbf{r}}_i^R(t') = \mathbf{F}_i(\{\mathbf{r}_j^R(t')\}) + v(\mathbf{r}_i^R(t'))\mathbf{u}_i^R(t').$$

Then, using that $\mathbf{r}_i(t) = \mathbf{r}_i^R(t_f - t)$ and $\dot{\mathbf{r}}_i(t) = -\dot{\mathbf{r}}_i^R(t_f - t)$, this implies

$$-\dot{\mathbf{r}}_i(t) = \mathbf{F}_i(\{\mathbf{r}_j(t)\}) + v(\mathbf{r}_i(t))\mathbf{u}_i^R(t_f - t). \quad (84)$$

Adding Eqs. (83) and (84) then leads to

$$0 = 2\mathbf{F}_i(\{\mathbf{r}_j(t)\}) + v(\mathbf{r}_i(t)) [\mathbf{u}_i^R(t_f - t) + \mathbf{u}_i(t)]. \quad (85)$$

If $\mathbf{F}_i(\{\mathbf{r}_j(t)\}) = 0$, Eq. (85) can be satisfied by setting $\mathbf{u}_i^R(t_f - t) = -\mathbf{u}_i(t)$; for a noninteracting system a time-reversed trajectory can be realized by flipping the orientation. On the other hand, if $\mathbf{F}_i(\{\mathbf{r}_j(t)\}) \neq 0$, it is impossible to satisfy Eq. (85) generically because

$$|\mathbf{u}_i^R(t_f - t)| = 1 \neq \left| -\frac{2\mathbf{F}_i(\{\mathbf{r}_j(t)\})}{v(\mathbf{r}_i(t))} - \mathbf{u}_i(t) \right|. \quad (86)$$

The required time-reversed orientation vector is typically not a unit vector, which violates the definition of the dynamics.

C. Momentum sources

Let us now show that, for interacting ABPs and RTPs in the presence of an activity landscape, momentum sources arise that allow the emergence of ratchet currents.

To do so, we start from Eq. (55) for the empirical distribution. We use the standard method of decomposing $\psi(\mathbf{r}, \mathbf{u})$ into a hierarchy of orientational modes given by the density $\hat{\rho}(\mathbf{r}) = \sum_i \delta(\mathbf{r} - \mathbf{r}_i)$, magnetization vector $\hat{\mathbf{m}}(\mathbf{r}) = \sum_i \mathbf{u}_i \delta(\mathbf{r} - \mathbf{r}_i)$, nematic order tensor $\hat{\mathbf{Q}}(\mathbf{r}) = \sum_i \delta(\mathbf{r} - \mathbf{r}_i) (\mathbf{u}_i \otimes \mathbf{u}_i - \frac{\mathbb{I}}{d})$, and so on [41]. For both ABPs and RTPs, we obtain for the average fields [63–68]

$$\dot{\rho} = -\nabla \cdot \left[\mathbf{m}v - \int d^d \mathbf{r}' \nabla U_{\text{int}}(\mathbf{r} - \mathbf{r}') \langle \hat{\rho}(\mathbf{r}) \hat{\rho}(\mathbf{r}') \rangle \right], \quad (87)$$

$$\dot{\mathbf{m}} = -\nabla \cdot \left[v \left(\mathbf{Q} + \mathbb{I} \frac{\rho}{d} \right) - \int d^d \mathbf{r}' \nabla U_{\text{int}}(\mathbf{r} - \mathbf{r}') \otimes \langle \hat{\mathbf{m}}(\mathbf{r}) \hat{\rho}(\mathbf{r}') \rangle \right] - \frac{\mathbf{m}}{\tau}. \quad (88)$$

(The dynamics of higher moments is not required here.) In steady state, we set $\partial_t \mathbf{m} = 0$ to get

$$\mathbf{m} \equiv -\tau \nabla \cdot \mathbf{J}_m, \quad (89)$$

where

$$\mathbf{J}_m = v \left(\mathbf{Q} + \mathbb{I} \frac{\rho}{d} \right) - \int d^d \mathbf{r}' \nabla U_{\text{int}}(\mathbf{r} - \mathbf{r}') \otimes \langle \hat{\mathbf{m}}(\mathbf{r}) \hat{\rho}(\mathbf{r}') \rangle \quad (90)$$

Making this substitution, and absorbing the mechanical forces in Eq. (87) into the Irving-Kirkwood stress $\boldsymbol{\sigma}_{\text{IK}}$ [47], we find

$$\begin{aligned} \dot{\rho} &= -\nabla \cdot \left\{ -\tau v(\mathbf{r}) \nabla \cdot \mathbf{J}_m + \nabla \cdot \boldsymbol{\sigma}_{\text{IK}} \right\} \\ &= -\nabla \cdot \left\{ \nabla \cdot \left[-\tau v \mathbf{J}_m + \boldsymbol{\sigma}_{\text{IK}} \right] + \tau [\nabla v(\mathbf{r})] \cdot \mathbf{J}_m \right\} \\ &\equiv -\nabla \cdot \left\{ \nabla \cdot \boldsymbol{\sigma}_{\text{tot}} + \delta \mathbf{F}_A \right\}. \end{aligned} \quad (91)$$

If the activity is constant, the active forces can be written as the divergence of an active stress, as expected [63]. However, variations in the self-propulsion speed lead to a nonconservative active force $\delta \mathbf{F}_A$, as identified in [67]. These forces cannot be written as the divergence of a local stress tensor, thus generating sinks and sources of momentum which, as we show below, can power steady-state currents.

D. Interaction-induced current

Interacting ABPs and RTPs in asymmetric activity landscapes thus violate TRS, parity symmetry, and momentum conservation, which generically allows for

ratchet currents. Let us now show how we can predict the emergence of such currents quantitatively using a perturbation theory in the interaction potential to solve Eqs. (87)-(88).

First, to make progress we use the factorization approximation

$$\langle \hat{\rho}(\mathbf{r}) \hat{\rho}(\mathbf{r}') \rangle = \langle \hat{\rho}(\mathbf{r}) \rangle \langle \hat{\rho}(\mathbf{r}') \rangle = \rho(\mathbf{r}) \rho(\mathbf{r}') \quad (92)$$

$$\langle \hat{\mathbf{m}}(\mathbf{r}) \hat{\rho}(\mathbf{r}') \rangle = \langle \hat{\mathbf{m}}(\mathbf{r}) \rangle \langle \hat{\rho}(\mathbf{r}') \rangle = \mathbf{m}(\mathbf{r}) \rho(\mathbf{r}'). \quad (93)$$

In this Curie-Weiss mean-field picture, the particles at position \mathbf{r} experience an effective potential $V_{\text{eff}}(\mathbf{r}) \equiv U_{\text{int}} * \rho(\mathbf{r})$ as in Eq. (39). Then, the dynamics boil down to those for an ABP/RTP in d dimensions moving in the activity landscape $v(\mathbf{r})$ and the potential landscape $V_{\text{eff}}(\mathbf{r})$. However, since the latter depends on ρ , these equations are nonlinear and should be solved self-consistently. As we now show, progress can be made in the limit of a weak interaction potential. We thus rewrite $U_{\text{int}} = \varepsilon \tilde{U}_{\text{int}}$ and work perturbatively in ε .

1. Leading-order ratchet current for ABPs and RTPs in d dimensions

The mean-field steady-state equations for ABPs and RTPs in d dimensions read $\nabla \cdot \mathbf{J} = 0$ with

$$\mathbf{J} = \mathbf{m}v - \varepsilon \rho \nabla (\tilde{U}_{\text{int}} * \rho), \quad (94)$$

$$\mathbf{m} = -\tau \nabla \cdot \left\{ v \left(\mathbf{Q} + \mathbb{I} \frac{\rho}{d} \right) - \varepsilon \mathbf{m} \otimes \nabla (\tilde{U}_{\text{int}} * \rho) \right\}. \quad (95)$$

We then consider a perturbative ansatz for all fields

$$\begin{aligned} \rho &= \sum_{k=0}^{\infty} \varepsilon^k \rho_k, & \mathbf{m} &= \sum_{k=0}^{\infty} \varepsilon^k \mathbf{m}_k, & \mathbf{Q} &= \sum_{k=0}^{\infty} \varepsilon^k \mathbf{Q}_k, \dots \\ \mathbf{J} &= \sum_{k=0}^{\infty} \varepsilon^k \mathbf{J}_k \end{aligned} \quad (96)$$

At zeroth order in ε , we find $\mathbf{J}_0 = \mathbf{m}_0 = 0$ and $\rho_0 \propto 1/v$, consistent with the result for noninteracting particles. At first order, Eqs. (94)-(95) imply

$$\mathbf{J}_1 = \mathbf{m}_1 v - \rho_0 \nabla (\tilde{U}_{\text{int}} * \rho_0), \quad (97)$$

$$\mathbf{m}_1 = -\tau \nabla \cdot \left\{ v \left(\mathbf{Q}_1 + \mathbb{I} \frac{\rho_1}{d} \right) \right\}. \quad (98)$$

These equations are not closed, since they involve \mathbf{Q}_1 . To make progress, we consider an effectively 1-dimensional activity landscape $v(\mathbf{r}) = v(x)$, as in Fig. 5. Then, by symmetry, the steady-state current has to satisfy $\mathbf{J}_1 = J_1 \hat{x}$, with J_1 a constant. Dividing Eq. (97) by $v(x)$ and integrating over space then leads to

$$J_1 = -\kappa^3 \int_0^L dx \int_0^L dx' \frac{\tilde{U}'_{\text{int}}(x-x')}{v(x)^2 v(x')}. \quad (99)$$

This prediction is plotted as the black curve in Fig. 5(c) and compared to the result of numerical simulations.

While it predicts the order of magnitude of J when the interaction strength is weak, the slope at $\varepsilon = 0$ slightly differs from that measured numerically, probably due to the factorization approximation in (92)-(93). It also misses the current reversal at larger values of ε .

Going to higher order in ε requires a closure in the moments of ψ , which can be done by taking a small $|\nabla v|$ limit. Alternatively, we here consider one-dimensional run-and-tumble particles for which the expansion can be carried out to arbitrary order without further approximations.

2. Run-and-Tumble Particles in 1D

We here detail the perturbation theory for the case of RTPs in $d = 1$, whose dynamics read

$$\dot{x}_i = v(x_i)u_i - \sum_j U'_{\text{int}}(x_i - x_j), \quad (100)$$

where the orientation $u_i \in \{-1, +1\}$ is randomized at rate $\alpha = \tau^{-1}$. These dynamics can be equivalently written for density and magnetization fields $\hat{\rho}(x) = \sum_i \delta(x - x_i)$ and $\hat{m}(x) = \sum_i u_i \delta(x - x_i)$ as coupled hydrodynamic equations

$$\dot{\rho} = -\partial_x \left[vm - \int dx' \langle \hat{\rho}(x) \hat{\rho}(x') \rangle U'_{\text{int}}(x - x') \right] \quad (101)$$

$$\dot{m} = -\partial_x \left[v\rho - \int dx' \langle \hat{m}(x) \hat{\rho}(x') \rangle U'_{\text{int}}(x - x') \right] - \frac{m}{\tau}. \quad (102)$$

Performing the mean-field factorization Eqs. (92)-(93) then yields

$$\dot{\rho} = -\partial_x \left[vm - \rho \partial_x (U_{\text{int}} * \rho) \right] \quad (103)$$

$$\dot{m} = -\partial_x \left[v\rho - m \partial_x (U_{\text{int}} * \rho) \right] - \frac{m}{\tau}. \quad (104)$$

The equations above are equivalent to RTP equations within an effective potential $V_{\text{eff}} \equiv U_{\text{int}} * \rho$. In fact, the steady-state for 1d RTPs in an arbitrary *external* force $f(x)$ (e.g., $f(x) = -V'(x)$) can be solved explicitly in the absence of interactions as detailed in Appendix D. As for PBPs, the resulting solution could then be used to determine the steady-state for *interacting* system by inserting $f(x) = -\partial_x V_{\text{eff}} = -\partial_x (U_{\text{int}} * \rho)$, and performing a self-consistent perturbation in the strength of U_{int} .

Here, we follow the more direct route of solving Eqs (103) and (104) perturbatively. We again denote the interaction potential as $U_{\text{int}} = \varepsilon \tilde{U}_{\text{int}}$ and expand the fields in powers of the ε :

$$\rho = \sum_{k=0}^{\infty} \varepsilon^k \rho_k, \quad m = \sum_{k=0}^{\infty} \varepsilon^k m_k, \quad J = \sum_{k=0}^{\infty} \varepsilon^k J_k. \quad (105)$$

We then solve the steady-state equations

$$J = vm - \varepsilon \rho \partial_x (\tilde{U}_{\text{int}} * \rho) \in \mathbb{R} \quad (106)$$

$$m = -\tau \partial_x \left[v\rho - \varepsilon m \partial_x (\tilde{U}_{\text{int}} * \rho) \right] \quad (107)$$

order-by-order in ε .

At 0th order, the solution reads

$$\rho_0(x) = \frac{\kappa_0}{v(x)}, \quad m_0(x) = 0, \quad J_0 = 0 \quad (108)$$

where $\kappa_0 = N \left[\int_0^L \frac{dx}{v(x)} \right]^{-1}$ ensures ρ_0 's normalization.

At 1st order, we find

$$\rho_1 = \frac{1}{\tau v} \left\{ \kappa_1 - \int_0^x \frac{dx}{v(x')} \left[J_1 + \frac{\kappa_0^2 (\tilde{U}_{\text{int}} * v^{-1})'(x')}{v(x')} \right] \right\}$$

$$m_1 = -\tau \partial_x (v\rho_1)$$

$$J_1 = -\kappa_0^3 \int_0^L dx \int_0^L dx' \frac{\tilde{U}'_{\text{int}}(x - x')}{v(x)^2 v(x')},$$

in agreement with Eq. (99). Once again, a ratchet current appears for a generic asymmetric $v(x)$.

This calculation can be carried to arbitrary order using the recursive relation

$$J_n = -\kappa_0 \sum_{k=0}^{n-1} \int_0^L dx \frac{\rho_k(x) (\tilde{U}_{\text{int}} * \rho_{n-k-1})'(x)}{v(x)}$$

$$\rho_n = \frac{\kappa_n}{v} + \frac{1}{v} \int_0^x dx' \left[\sum_{k=0}^{n-1} m_k (\tilde{U}_{\text{int}} * \rho_{n-k-1})' - \frac{m_n}{\tau} \right]$$

$$m_n = \frac{J_n}{v} + \sum_{k=0}^{n-1} \rho_k (\tilde{U}_{\text{int}} * \rho_{n-k-1})'.$$

The result of this procedure is illustrated in Fig. 6 (to order 6). It agrees very well with numerical simulations in the high-density limit where the factorization approximation is expected to work best.

E. Summary

ABPs and RTPs in parity-breaking activity landscapes do not exhibit steady-state currents in the absence of interactions. While this appears to violate the ratchet principle, since active matter is out of thermal equilibrium, we have shown that the particles obey detailed balance with respect to their non-Boltzmann steady-state measures in position space. This effective TRS thus forbids a ratchet current in the non-interacting case.

In the presence of interactions, TRS is violated and the systems do not admit a generalized stress tensor, so that nonconservative forces can act as momentum sources, leading to steady-state currents. We have seen these currents borne out numerically, and characterized their emergence analytically employing a mean-field factorization approximation [Figs. 5 and 6].

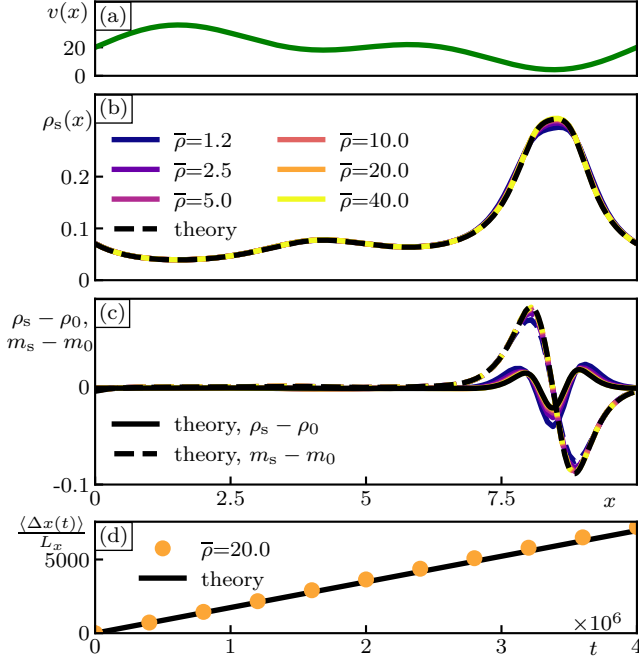


FIG. 6. **Interacting RTPs in 1d.** (a) Activity landscape $v(x)$. (b) Steady-state density profile $\rho_s(x)$ as the average density $\bar{\rho}$ is varied. The dashed black line corresponds to the theoretical prediction to order 6 in the perturbation theory. (c) Detailed comparison of the convergence between numerics and theory as $\bar{\rho}$ is increased for the density (solid) and orientation (dashed) fields. (d) Average displacement per particle (symbol) compared to the theoretical prediction (solid line). Numerical details are given in Appendix A 4.

In the mean-field picture, the mechanism behind the interaction-induced current is the coupling between the activity landscape and the effective potential that each particle experiences from its neighbors.

V. ACTIVE ORNSTEIN-UHLENBECK PARTICLES

Finally, we consider another frequently-studied active model called Active Ornstein-Uhlenbeck Particles (AOUPs), which, as we show below, offers interesting differences with respect to ABPs and RTPs. We consider N particles evolving in d dimensions according to

$$\dot{\mathbf{r}}_i = \mathbf{v}_i - \sum_j \nabla U_{\text{int}}(\mathbf{r}_i - \mathbf{r}_j), \quad (109)$$

$$\tau \dot{\mathbf{v}}_i = -\mathbf{v}_i + \sqrt{2D(\mathbf{r}_i)} \boldsymbol{\eta}_i(t), \quad (110)$$

where $\boldsymbol{\eta}_i(t)$ is a centered Gaussian white noise satisfying $\langle \eta_{i,\mu}(t) \rangle = 0$ and $\langle \eta_{i,\mu}(t) \eta_{j,\nu}(t') \rangle = \delta_{ij} \delta_{\mu\nu} \delta(t - t')$. In Eq. (110), the large-scale diffusivity $D(\mathbf{r})$ makes the AOUP activity vary in space.

We consider the empirical density of particles in the position-propulsion-velocity space $\hat{\psi}(\mathbf{r}, \mathbf{v}, t) \equiv \sum_i \delta(\mathbf{r}_i -$

$\mathbf{r}) \delta(\mathbf{v}_i - \mathbf{v})$. The equation describing the dynamics of its average, $\psi(\mathbf{r}, \mathbf{v}) = \langle \hat{\psi}(\mathbf{r}, \mathbf{v}) \rangle$, is

$$\begin{aligned} \dot{\psi}(\mathbf{r}, \mathbf{v}, t) = & \frac{1}{\tau} \nabla_{\mathbf{v}} \cdot \left[\mathbf{v} \psi + \frac{D(\mathbf{r})}{\tau} \nabla_{\mathbf{v}} \psi \right] - \nabla \cdot \left[\mathbf{v} \psi \right. \\ & \left. - \int d^d \mathbf{r}' \int d^d \mathbf{v}' \nabla U_{\text{int}}(\mathbf{r} - \mathbf{r}') \langle \hat{\psi}(\mathbf{r}, \mathbf{v}) \hat{\psi}(\mathbf{r}', \mathbf{v}') \rangle \right]. \end{aligned} \quad (111)$$

Ratchet currents have been shown to be forbidden for noninteracting AOUPs in one-dimensional activity landscapes $D(x)$ [26], a result we generalize below to the d -dimensional case. Noting that TRS is violated for AOUPs with spatially-varying activity, both with and without interactions [69], we demonstrate that, somewhat surprisingly, interaction-induced ratchet currents are forbidden in AOUPs. As for U-PBPs, this stems from an effective bulk momentum conservation. To demonstrate these results, we provide an exact expression for the generalized stress tensor, which forbids the momentum sources required to generate steady-state currents.

A. Numerics and phenomenology

The results of particle-based simulations of AOUPs in $d = 2$ space dimensions, with an effectively one-dimensional activity landscape $D(x)$, are reported in Fig. 7. The density distribution in the non-interacting case is distinct from its $\tau \rightarrow 0$ limit $\rho_s(x) \propto 1/D(x)$. This is further deformed by adding repulsive interactions between the particles, which flatten the density [Fig. 7(b)]. There is no ratchet current in interacting AOUPs, as evidenced by tracking the integrated particle displacements over time [Fig. 7(c)]. The generalized stress tensor of AOUPs is measured and characterized in Fig. 7d-f to illustrate the derivations of Sec. V C.

B. Time-reversal symmetry

In the absence of interactions, the dynamics for AOUPs [Eqs. (109)-(110)] is identical to the dynamics for underdamped PBPs [Eq. (2)], if τ is replaced by $1/\gamma$ and $D(\mathbf{r})$ is replaced by $T(\mathbf{r})/\gamma$. As discussed in Sec. II B, U-PBPs with spatially-varying temperature have nonzero EPR. The same thus holds for the equivalent system of AOUPs with spatially varying D . Consequently, AOUPs are “genuine” exceptions to the historical ratchet principle, violating both TRS and parity symmetry while lacking a current.

Like all other systems considered in this paper, adding interactions creates new mechanisms for entropy production. We calculate this directly in Appendix. E, where

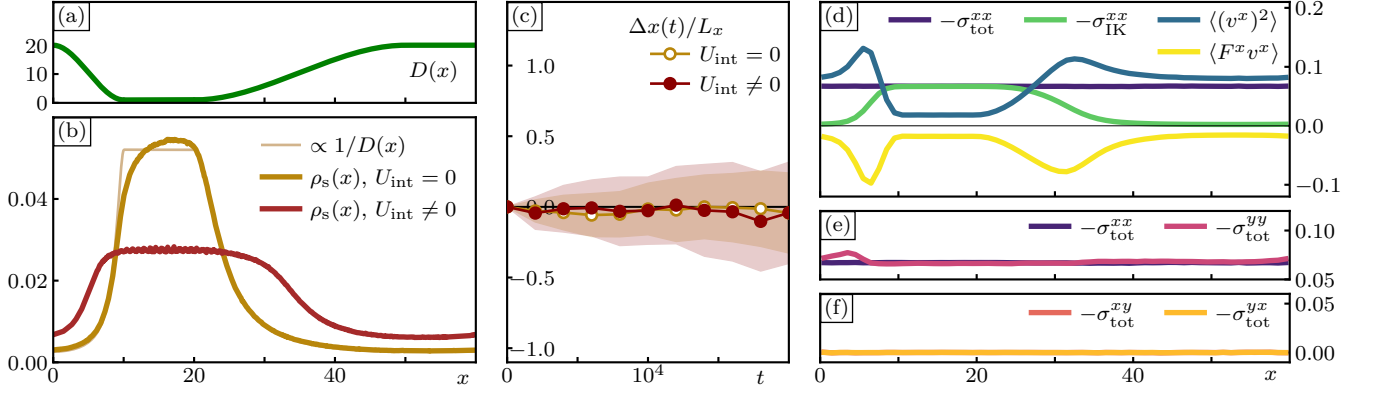


FIG. 7. **AOUPs are protected from a ratchet current by an emergent momentum conservation.** (a) The activity landscape $D(x)$ used in simulations. (b) The steady-state density distribution of AOUPs both without interactions (gold) and with interactions (dark red). The density in the $\tau \rightarrow 0$ limit, $\propto 1/D(x)$, is shown for reference (thin beige line). (c) Directly measuring the net particle displacement over time, both without and with interactions, reveals the absence of ratchet current. (d) Remarkably, AOUPs possess steady-state momentum conservation, so that gradients of active stresses $\tau \langle \mathbf{v}_i \otimes \mathbf{v}_i \rangle$ (blue) and $\tau \langle \mathbf{F}_i \otimes \mathbf{v}_i \rangle$ (yellow) are balanced by gradients in the Irving-Kirkwood stress (green). (e) The (y, y) stress σ_{tot}^{yy} is spatially varying unlike σ_{tot}^{xx} ; however it is constant along y by translational symmetry, thus generating no current. (f) All off-diagonal components of the stress are zero. Simulation details are provided in Appendix A 5.

we show the EPR field to be given by:

$$\hat{\sigma}(\mathbf{r}) = \sum_i \frac{\delta(\mathbf{r} - \mathbf{r}_i)}{D(\mathbf{r}_i)} \left[\sum_j \mathbf{f}_{\text{int}}(\mathbf{r}_i - \mathbf{r}_j) - \tau \ddot{\mathbf{r}}_i \right] \cdot \left[\dot{\mathbf{r}}_i - \tau \sum_j (\dot{\mathbf{r}}_i - \dot{\mathbf{r}}_j) \cdot \nabla \mathbf{f}_{\text{int}}(\mathbf{r}_i - \mathbf{r}_j) \right]. \quad (112)$$

Note that the last term of the second bracket does not appear in the EPR field of U-PBPs, Eq. (8), and is thus unique to interactions between AOUPs.

C. Momentum conservation

We now project Eq. (111) onto a hierarchy of orientational modes given by the density $\hat{\rho}(\mathbf{r}) = \sum_i \delta(\mathbf{r} - \mathbf{r}_i)$, magnetization vector $\hat{\mathbf{m}}(\mathbf{r}) = \sum_i \mathbf{v}_i \delta(\mathbf{r} - \mathbf{r}_i)$, nematic order tensor $\hat{\mathbf{Q}}(\mathbf{r}) = \sum_i \delta(\mathbf{r} - \mathbf{r}_i) (\mathbf{v}_i \otimes \mathbf{v}_i - \mathbb{I} \frac{D(\mathbf{r}_i)}{\tau})$. As a result, we find

$$\dot{\rho} = -\nabla \cdot \left[\mathbf{m} + \int d^d \mathbf{r}' \mathbf{f}_{\text{int}}(\mathbf{r} - \mathbf{r}') \langle \hat{\rho}(\mathbf{r}) \hat{\rho}(\mathbf{r}') \rangle \right] \quad (113)$$

$$\dot{\mathbf{m}} = -\nabla \cdot \mathbf{J}_m - \mathbf{m}/\tau, \quad (114)$$

where

$$\mathbf{J}_m \equiv \mathbf{Q} + \mathbb{I} \frac{\rho D}{\tau} + \langle \hat{\mathbf{m}} \otimes (\mathbf{f}_{\text{int}} * \hat{\rho}) \rangle. \quad (115)$$

In the steady state, $\dot{\mathbf{m}} = 0$ so that $\mathbf{m} = -\tau \nabla \cdot \mathbf{J}_m$. By recognizing that Eq. (113) has the structure of a continuity equation, $\dot{\rho} = -\nabla \cdot \mathbf{J}$, in the steady state we express the current as the divergence of a stress tensor as

$$\mathbf{J} = -\nabla \cdot [\tau \mathbf{J}_m - \boldsymbol{\sigma}_{\text{IK}}] = \nabla \cdot \boldsymbol{\sigma}_{\text{tot}} \quad (116)$$

where $\boldsymbol{\sigma}_{\text{IK}}$ is the Irving-Kirkwood stress tensor [47].

In Fig. 7(e) and (f), we plot each component of the AOUPs stress tensor measured in particle-based simulations. Note that both off-diagonal components are zero: $\boldsymbol{\sigma}_{\text{tot}}^{xy} = \boldsymbol{\sigma}_{\text{tot}}^{yx} = 0$. We analyze the (x, x) component in detail as it determines the current flowing toward the x -direction. From Eq. (116), we obtain

$$\boldsymbol{\sigma}_{\text{tot}}^{xx} = \boldsymbol{\sigma}_{\text{IK}}^{xx} - \sum_i [\tau \langle v_i^x \otimes v_i^x \rangle + \tau \langle v_i^x \otimes F_i^x \rangle],$$

where $F_i^x = -\sum_j \partial_{x_i} U_{\text{int}}(\mathbf{r}_i - \mathbf{r}_j)$ is the force experienced by particle i along \hat{x} . Our measurements show that the active stresses, $-\tau \langle \mathbf{v}_i \otimes \mathbf{v}_i \rangle$ and $-\tau \langle \mathbf{F}_i \otimes \mathbf{v}_i \rangle$, and the passive one, $\boldsymbol{\sigma}_{\text{IK}}$, balance each other, resulting in a constant total stress and a flux-free steady state. Interestingly, the (y, y) component of the total stress is not constant with respect to x . This does not affect the current since $\mathbf{J} = \hat{x} \partial_x \boldsymbol{\sigma}_{\text{tot}}^{xx} + \hat{y} \partial_y \boldsymbol{\sigma}_{\text{tot}}^{yy}$ and $\partial_y \boldsymbol{\sigma}_{\text{tot}}^{yy} = 0$.

Our generalized stress tensor is also useful to pinpoint similarities and differences between AOUPs and U-PBPs. Comparing Eq. (116) with the U-PBP stress tensor (14), we find

$$\boldsymbol{\sigma}_{\text{U-PBP}} = \frac{1}{\gamma} [\boldsymbol{\sigma}_{\text{IK}} - \mathbf{Q} - \mathbb{I} \rho T], \quad (117)$$

$$\boldsymbol{\sigma}_{\text{AOUP}} = \tau \left[\boldsymbol{\sigma}_{\text{IK}} - \mathbf{Q} - \mathbb{I} \frac{\rho D}{\tau} - \langle \hat{\mathbf{m}} \otimes (\mathbf{f}_{\text{int}} * \rho) \rangle \right]. \quad (118)$$

They are almost identical under the mapping that identifies $\mathbf{p} \leftrightarrow \mathbf{v}$, $1/\gamma \leftrightarrow \tau$, and $T \leftrightarrow D/\tau$. The final term captures the fundamental differences between AOUPs and U-PBPs, which results from the different ways pairwise forces enter the dynamics. Interestingly this difference

impacts fundamental properties such as the existence of MIPS or lack thereof, but not the absence of ratchet currents.

D. Summary

Despite their apparent similarities, the contrast between ABPs/RTPs and AOUPs is striking when it comes to interaction-induced ratchet currents. While ABPs and RTPs display interaction-induced currents in activity landscapes (Fig. 5), this is impossible for AOUPs. This is because, surprisingly, AOUPs with spatially varying activity admit a generalized stress tensor.

VI. DISCUSSION AND CONCLUSION

In this work, we have considered a series of stochastic particle systems for which we have shown that the emergence of ratchet currents requires the systematic violation of TRS, parity symmetry, and bulk momentum conservation.

By considering overdamped and underdamped Brownian particles as well as ABPs, RTPs, and AOUPs, we have shown that the litmus test for the emergence of interaction-induced ratchet currents in fluctuation landscapes is not activity. The existence of an effective momentum conservation law is thus a new dividing line between non-equilibrium systems that raises new questions. In particular, we have here focused on continuous diffusion models in space and the question as to how our results extend to more general Markov processes, multi-state systems, or lattice gases is open. The notion of effective momentum conservation does not easily generalize to such cases and the identification of the possible symmetries and conservation laws that may prevent the emergence of ratchet currents in these contexts is an exciting open question for future work.

Acknowledgements. We thank Hughes Chate, Yariv Kafri, Jeremy O’Byrne, and Vivien Lecomte for insightful discussions.

Appendix A: Simulation details

All simulations are run with periodic boundary conditions in all directions, using a standard Euler(-Maruyama) discretization scheme. All interacting simulations were done using the soft repulsive harmonic potential and force given by:

$$U_{\text{int}}(\mathbf{r}) = \frac{\varepsilon r_{\text{int}}}{2} \left[1 - \frac{|\mathbf{r}|}{r_{\text{int}}} \right]^2 \equiv \varepsilon \tilde{U}_{\text{int}}(\mathbf{r}), \quad (\text{A1})$$

$$\mathbf{f}_{\text{int}}(\mathbf{r}) = -\nabla U_{\text{int}}(\mathbf{r}) = \varepsilon \frac{\mathbf{r}}{|\mathbf{r}|} \left[1 - \frac{|\mathbf{r}|}{r_{\text{int}}} \right]. \quad (\text{A2})$$

Our unit of length are such that the interaction range is $r_{\text{int}} = 1$. For the ABP, RTP, and AOUP simulations, time units are such that $\tau = 1$ (with $\tau = \alpha^{-1}$ for RTPs and $\tau = D_r^{-1}$ for ABPs). For PBP simulations, the mobility or inverse damping is similarly set to $\mu = \gamma^{-1} = 1$.

All activity, diffusivity, and temperature landscapes presented in this paper, with the exception of those used in Figs. 1, 6, and 8, are constructed using cubic interpolation between some minimum and maximum values. More precisely, consider a landscape $f(x)$ ranging from f_0 to f_1 using reference points $x_\ell < x_{c1} \leq x_{c2} < x_r$. Define the interpolation distances $\Delta x_1 \equiv x_{c1} - x_\ell$ and $\Delta x_2 \equiv x_r - x_{c2}$, and the length of the central segment $\Delta x_c \equiv x_{c2} - x_{c1}$. Then f has the functional form

$$f(x) = \begin{cases} f_1, & x \in [0, x_\ell] \cup [x_r, L_x] \\ f_0, & x \in [x_{c1}, x_{c2}] \\ f_1 + (f_0 - f_1)s\left(\frac{x-x_\ell}{\Delta x_1}\right), & x \in [x_\ell, x_{c1}] \\ f_0 + (f_1 - f_0)s\left(\frac{x-x_{c2}}{\Delta x_2}\right), & x \in [x_{c2}, x_r], \end{cases} \quad (\text{A3})$$

$$s(x) \equiv -2x^3 + 3x^2. \quad (\text{A4})$$

Note that while our analytic calculations often use the normalization $\int d^d \mathbf{r} \rho(\mathbf{r}) = N$, our figures display simulation data that is normalized such that $\int d^d \mathbf{r} \rho(\mathbf{r}) = 1$, for ease of comparison with non-interacting systems of $N = 1$.

Below, we describe the simulations presented in the figures in the main text. A summary of these parameters is given in Table II.

1. Fig. 1

The simulations shown in Fig. 1 were performed using $N = 200$ particles (AOUPs and ABPs on the left and right panels, respectively) with interaction strength $\varepsilon = 5$. The domain has size $L_x = 8$ and $L_y = 6$. The activity landscape is of the form

$$v(\mathbf{r}) = D(\mathbf{r}) = \sum_{n,m=1}^4 A_{nm} \cos \left[2\pi \left(\frac{nx}{L_x} + B_{nm} \right) \right] \times \cos \left[2\pi \left(\frac{ny}{L_y} + C_{nm} \right) \right] \quad (\text{A5})$$

where A_{nm} , B_{nm} , and C_{nm} are arbitrarily-chosen 4×4 matrices. The activity falls within the range $D(\mathbf{r}), v(\mathbf{r}) \in [0.009, 2.4]$.

2. Underdamped Passive Brownian Particles (Fig. 2)

The simulations shown in Fig. 2 were performed using $N = 700$ particles with interaction strength $\varepsilon = 0$

Fig.	N	L_x	L_y	f_0	f_1	Δx_1	Δx_c	Δx_2	ε	dt	t_f	n_{seed}	notes
1	200	8	6	-	-	-	-	-	5	10^{-3}	10^6	80	2d sinusoidal $v(\mathbf{r})$, $D(\mathbf{r})$
2	700	60	15	20	1	10	10	30	{0, 50}	2.5×10^{-4}	2×10^4	30	$\alpha \in \{0, 0.125, \dots, 1\}$
3	200	20	5	20	1	2.5	0	17.5	50	2.5×10^{-4}	2×10^5	200	
4	400	50	15	20	1	8	9	24	50	5×10^{-4}	10^5	1	
5	500	20	5	20	1	2.5	2.5	7	{0, 0.025, ..., 0.225}	5×10^{-4}	2×10^4	400	1d sinusoidal $v(x)$
6	{12, 25, ..., 400}	10	-	-	-	-	-	-	$15/N$	5×10^{-4}	varies	varies	
7	700	60	15	20	1	10	10	30	{0, 50}	2.5×10^{-4}	2×10^4	30	1d sinusoidal $v(x)$, $U(x)$
8	1	20	-	-	-	-	-	-	0	10^{-3}	10^3	96,000	

TABLE II. Simulation parameters for each figure. All but Fig. 1 have translational symmetry in all but the x dimension. All but Figs. 6 and 8 are in 2 space dimensions. All but Figs. 1, 6, and 8 use a fluctuation landscape $f(x)$ that interpolates cubically between the values f_0 to f_1 [Eq. (A3)].

(gold lines) and $\varepsilon = 50$ (dark red lines). The domain has size $L_x = 60$ and $L_y = 15$. The temperature ranges from $T_0 = 1$ to $T_1 = 20$. The temperature field is constructed as in Eq. (A3) with reference points $x_\ell = 0$, $x_{c1} = 10$, $x_{c2} = 20$, $x_r = 50$.

3. Overdamped Passive Brownian Particles (Figs. 3-4)

The simulations shown in Fig. 3 were performed using $N = 200$ particles with interaction strength $\varepsilon = 50$. The domain has size $L_x = 20$ and $L_y = 5$. The temperature ranges from $T_0 = 1$ to $T_1 = 20$. The temperature field is constructed as in Eq. (A3) with reference points $x_\ell = 0$, $x_{c1} = x_{c2} = 2.5$, $x_r = L_x$.

Simulations of OD PBP with discretization $\alpha \neq 0$ were performed with the same Euler discretization, which corresponds to an Itô process, and varying the corresponding spurious drift [52]:

$$\dot{\mathbf{r}}_i \stackrel{\alpha}{=} \mathbf{F}_i(\{\mathbf{r}_j\}) + \sqrt{2T(\mathbf{r}_i)}\boldsymbol{\eta}_i \quad (\text{A6})$$

$$\Leftrightarrow \dot{\mathbf{r}}_i \stackrel{0}{=} \mathbf{F}_i(\{\mathbf{r}_j\}) + \alpha \nabla T(\mathbf{r}_i) + \sqrt{2T(\mathbf{r}_i)}\boldsymbol{\eta}_i. \quad (\text{A7})$$

The simulations shown in Fig. 4 were performed using $N = 400$ particles with interaction strength $\varepsilon = 50$. The domain has size $L_x = 50$ and $L_y = 15$. The temperature ranges from $T_0 = 1$ to $T_1 = 10$ with the reference points of Eq. (A3) given by $x_\ell = 0$, $x_{c1} = 8$, $x_{c2} = 17$, $x_r = 41$. The EPR profile was measured using 2×10^7 equally-spaced time samples.

4. Active Brownian and Run-and-Tumble Particles (Figs. 5-6, 8)

The simulations shown in Fig. 5 were each performed using $N = 500$ particles with interaction strengths $\varepsilon \in \{0, 0.025, 0.05, \dots, 0.225\}$. The domain has size $L_x =$

20 and $L_y = 5$. The activity ranged from $v_0 = 1$ to $v_1 = 20$ with the reference points of Eq. (A3) given by $x_\ell = 0$, $x_{c1} = 2.5$, $x_{c2} = 5$, $x_r = 12$.

The simulations shown in Fig. 6 involved interacting 1d RTPs with sinusoidal activity profile $v(x) = 20 \left[0.5 \sin\left(\frac{2\pi x}{L_x}\right) + 0.4 \sin\left(\frac{4\pi x}{L_x}\right) \right]$. Different simulations were run with different numbers of particles $N \in \{12, 25, 50, 100, 200, 400\}$. The interaction strengths ε are chosen such that $N\varepsilon = 15$. The simulation lengths t_f and number of seeds n_{seed} vary with the number of particles N as indicated in the following list of tuples $(N, t_f, n_{\text{seed}})$: $(12, 6 \times 10^7, 480)$, $(25, 6 \times 10^7, 240)$, $(50, 5 \times 10^7, 400)$, $(100, 8 \times 10^6, 240)$, $(200, 4 \times 10^6, 360)$, and $(400, 2 \times 10^6, 400)$.

The simulations shown in Fig. 8 involved 96,000 independent RTPs in a 1-dimensional domain of size $L = 20$. The activity and potential landscapes $v(x)$ and $U(x)$ were constructed as the sum of 12 Fourier modes,

$$v(x) = \sum_{n=1}^{12} a_n \sin(2\pi(nx/L + \phi_n)) \quad (\text{A8})$$

$$U(x) = \sum_{n=1}^{12} b_n \sin(2\pi(nx/L + \psi_n)). \quad (\text{A9})$$

They ran until the time $t_f = 1000$, with a timestep $dt = 10^{-3}$.

5. Active Ornstein Uhlenbeck Particles (Fig. 7)

The simulations shown in Fig. 7 were performed using $N = 700$ particles with interaction strength $\varepsilon = 0$ (gold lines) and $\varepsilon = 50$ (dark red lines). The domain has size $L_x = 60$ and $L_y = 15$. The diffusivity ranges from $D_0 = 1$ to $D_1 = 20$. The temperature field is constructed as in Eq. (A3) with reference points $x_\ell = 0$, $x_{c1} = 10$, $x_{c2} = 20$, $x_r = 50$.

Appendix B: EPR for interacting U-PBPs in temperature fields

Here we provide a detailed calculation of the EPR given in Eq. (8) for interacting U-PBPs in an inhomogeneous temperature field. We calculate this by directly computing the probability of a trajectory with dynamics defined in Eq. (2), conditioned on the particles' starting positions and momenta. While no discretization ambiguity afflicts these dynamics, treating the discretization carefully is necessary when calculating path probabilities. Thus, we define the discretized timesteps $t_k = k\Delta t$ for $k \in \{0, 1, \dots, M\}$ where $M\Delta t = t_f$. We also consider a Stratonovich-discretized version of the dynamics in position space and thus introduce the position at the midpoint of the timestep k ,

$$\bar{\mathbf{r}}_i^k \equiv \frac{\mathbf{r}_i^k + \mathbf{r}_i^{k+1}}{2}, \quad (\text{B1})$$

and the spatial increments

$$\Delta \mathbf{r}_i^k \equiv \mathbf{r}_i^{k+1} - \mathbf{r}_i^k. \quad (\text{B2})$$

Starting from the continuous-time dynamics

$$\dot{\mathbf{r}}_i = -\gamma \dot{\mathbf{r}}_i + \sum_{j=1}^N \mathbf{f}_{\text{int}}(\mathbf{r}_i - \mathbf{r}_j) + \sqrt{2\gamma T(\mathbf{r}_i)} \boldsymbol{\eta}_i, \quad (\text{B3})$$

the discretized dynamics reads

$$\begin{aligned} \frac{\Delta \mathbf{r}_i^{k+1} - \Delta \mathbf{r}_i^k}{\Delta t^2} &= -\gamma \left(\frac{\Delta \mathbf{r}_i^k}{\Delta t} \right) + \sum_{j=1}^N \mathbf{f}_{\text{int}}(\bar{\mathbf{r}}_i^k - \bar{\mathbf{r}}_j^k) \\ &\quad + \sqrt{2\gamma T(\bar{\mathbf{r}}_i^k)} \Delta \boldsymbol{\eta}_i^{k+1}, \end{aligned} \quad (\text{B4})$$

where $\Delta \boldsymbol{\eta}_i^{k+1}$ is a centered Gaussian noise that satisfies $\langle \Delta \eta_{i,\mu}^k \Delta \eta_{j,\nu}^\ell \rangle = \delta_{ij} \delta_{\mu\nu} \delta_{k,\ell} / \Delta t$. We know the probability of a noise trajectory,

$$\mathbb{P}[\{\Delta \boldsymbol{\eta}_i^k\} | \{\mathbf{r}_i^0, \mathbf{r}_i^1\}] \propto \exp \left[- \sum_{i=1}^N \sum_{k=1}^{M-1} \frac{\Delta t}{2} |\Delta \boldsymbol{\eta}_i^k|^2 \right], \quad (\text{B5})$$

from which the probabilities of the spatial trajectories can be found using the equality

$$\mathbb{P}[\{\mathbf{r}_i^k\} | \{\mathbf{r}_i^0, \mathbf{r}_i^1\}] = \mathbb{P}[\{\Delta \boldsymbol{\eta}_i^k\} | \{\mathbf{r}_i^0, \mathbf{r}_i^1\}] \left| \frac{\mathbb{D}[\{\Delta \boldsymbol{\eta}_i^k\} | \{\mathbf{r}_i^0, \mathbf{r}_i^1\}]}{\mathbb{D}[\{\mathbf{r}_i^k\} | \{\mathbf{r}_i^0, \mathbf{r}_i^1\}]} \right| \quad (\text{B6})$$

where $|\mathbb{D}[\{\Delta \boldsymbol{\eta}_i^k\} | \{\mathbf{r}_i^0, \mathbf{r}_i^1\}] / \mathbb{D}[\{\mathbf{r}_i^k\} | \{\mathbf{r}_i^0, \mathbf{r}_i^1\}]|$ is the Jacobian between the $M-1$ variables $\{\Delta \boldsymbol{\eta}_i^k\}_{k=1}^{M-1}$ and the

$M-1$ variables $\{\mathbf{r}_i^k\}_{k=2}^M$. Note the shift in k indices: $\Delta \boldsymbol{\eta}_i^k$ determines \mathbf{r}_i^{k+1} . Note that we condition on the positions in the first two timesteps, $\{\mathbf{r}_i^0, \mathbf{r}_i^1\}$, which is equivalent to conditioning on the initial positions and momenta. We first note, using the relation between the variables given by Eq. (B4), that this Jacobian will be upper triangular in the time dimension, because

$$\frac{\partial \Delta \eta_{i,\mu}^{k+1}}{\partial r_{j,\nu}^\ell} = 0 \quad \text{whenever } \ell > k+2. \quad (\text{B7})$$

For the diagonal elements $\partial \Delta \eta_{i,\mu}^{k+1} / \partial r_{j,\nu}^{k+2}$, we have

$$\frac{\delta_{ij} \delta_{\mu\nu}}{\Delta t^2} = \sqrt{2\gamma T(\bar{\mathbf{r}}_i^k)} \frac{\partial \Delta \eta_{i,\mu}^{k+1}}{\partial r_{j,\nu}^{k+2}} \quad (\text{B8})$$

from which we find the determinant

$$\left| \frac{\mathbb{D}[\{\Delta \boldsymbol{\eta}_i^k\} | \{\mathbf{r}_i^0, \mathbf{r}_i^1\}]}{\mathbb{D}[\{\mathbf{r}_i^k\} | \{\mathbf{r}_i^0, \mathbf{r}_i^1\}]} \right| = \prod_{k=0}^{M-2} \prod_{i=1}^N \frac{1}{\Delta t^2 \sqrt{2\gamma T(\bar{\mathbf{r}}_i^k)}} \quad (\text{B9})$$

$$\propto \prod_{k=0}^{M-2} \prod_{i=1}^N \frac{1}{\sqrt{T(\bar{\mathbf{r}}_i^k)}}. \quad (\text{B10})$$

Next, we convert the noise probability [Eq. (B5)] into spatial coordinates using Eq. (B4):

$$\begin{aligned} \mathbb{P}[\{\Delta \boldsymbol{\eta}_i^k\} | \{\mathbf{r}_i^0, \mathbf{r}_i^1\}] &\quad (\text{B11}) \\ \propto \exp \left[- \sum_{i=1}^N \sum_{k=0}^{M-2} \frac{\Delta t}{4\gamma T(\bar{\mathbf{r}}_i^k)} \left| \frac{\Delta \mathbf{r}_i^{k+1} - \Delta \mathbf{r}_i^k}{\Delta t^2} \right. \right. \\ &\quad \left. \left. + \gamma \frac{\Delta \mathbf{r}_i^k}{\Delta t} - \sum_{j=1}^N \mathbf{f}_{\text{int}}(\bar{\mathbf{r}}_i^k - \bar{\mathbf{r}}_j^k) \right|^2 \right]. \end{aligned}$$

Equations (B6), (B9), and (B11) give the trajectory probability density.

We wish to compare the probability of observing a trajectory to the probability of observing its time-reversed counterpart, to isolate the ‘‘time-irreversible parts’’ of the dynamics. We use the definition a trajectory's time-reverse \mathbf{r}_i^R

$$\mathbf{r}_i^{R,k} \equiv \mathbf{r}_i^{M-k}, \quad (\text{B12})$$

which satisfies $\bar{\mathbf{r}}_i^{R,k} = \bar{\mathbf{r}}_i^{M-k-1}$ and $\Delta \mathbf{r}_i^{R,k} = -\Delta \mathbf{r}_i^{M-k-1}$. We find the ratio between the probabilities of observing a trajectory and its reverse as:

$$\begin{aligned}
\frac{\mathbb{P}[\{\mathbf{r}_i^k\}|\{\mathbf{r}_i^0, \mathbf{r}_i^1\}]}{\mathbb{P}[\{\mathbf{r}_i^{R,k}\}|\{\mathbf{r}_i^{R,0}, \mathbf{r}_i^{R,1}\}]} &= \sqrt{\frac{T(\bar{\mathbf{r}}_i^{M-1})T(\bar{\mathbf{r}}_i^{M-2})}{T(\bar{\mathbf{r}}_i^0)T(\bar{\mathbf{r}}_i^1)}} \exp \left[- \sum_{i=1}^N \sum_{k=0}^{M-2} \left\{ \frac{\Delta t}{4\gamma T(\bar{\mathbf{r}}_i^k)} \left| \frac{\Delta \mathbf{r}_i^{k+1} - \Delta \mathbf{r}_i^k}{\Delta t^2} + \gamma \frac{\Delta \mathbf{r}_i^k}{\Delta t} - \sum_{j=1}^N \mathbf{f}_{\text{int}}(\bar{\mathbf{r}}_i^k - \bar{\mathbf{r}}_j^k) \right|^2 \right. \right. \\
&\quad \left. \left. - \frac{\Delta t}{4\gamma T(\bar{\mathbf{r}}_i^{M-k-1})} \left| \frac{-\Delta \mathbf{r}_i^{M-k-2} + \Delta \mathbf{r}_i^{M-k-1}}{\Delta t^2} - \gamma \frac{\Delta \mathbf{r}_i^{M-k-1}}{\Delta t} - \sum_{j=1}^N \mathbf{f}_{\text{int}}(\bar{\mathbf{r}}_i^{M-k-1} - \bar{\mathbf{r}}_j^{M-k-1}) \right|^2 \right\} \right] \\
&= \sqrt{\frac{T(\bar{\mathbf{r}}_i^{M-1})T(\bar{\mathbf{r}}_i^{M-2})}{T(\bar{\mathbf{r}}_i^0)T(\bar{\mathbf{r}}_i^1)}} \exp \left[- \sum_{i=1}^N \sum_{k=0}^{M-2} \frac{\Delta t}{4\gamma T(\bar{\mathbf{r}}_i^k)} \left| \frac{\Delta \mathbf{r}_i^{k+1} - \Delta \mathbf{r}_i^k}{\Delta t^2} + \gamma \frac{\Delta \mathbf{r}_i^k}{\Delta t} - \sum_{j=1}^N \mathbf{f}_{\text{int}}(\bar{\mathbf{r}}_i^k - \bar{\mathbf{r}}_j^k) \right|^2 \right. \\
&\quad \left. + \sum_{i=1}^N \sum_{k=1}^{M-1} \frac{\Delta t}{4\gamma T(\bar{\mathbf{r}}_i^k)} \cdot \left| \frac{\Delta \mathbf{r}_i^k - \Delta \mathbf{r}_i^{k-1}}{\Delta t^2} - \gamma \frac{\Delta \mathbf{r}_i^k}{\Delta t} - \sum_{j=1}^N \mathbf{f}_{\text{int}}(\bar{\mathbf{r}}_i^k - \bar{\mathbf{r}}_j^k) \right|^2 \right], \tag{B13}
\end{aligned}$$

where, in the second equality, we have relabelled the time indices for the backward path as $M - k - 1 \rightarrow k$. In the last line of Eq. (B13), we may replace $\frac{\Delta \mathbf{r}_i^k - \Delta \mathbf{r}_i^{k-1}}{\Delta t^2}$ with $\frac{\Delta \mathbf{r}_i^{k+1} - \Delta \mathbf{r}_i^k}{\Delta t^2}$, since their difference is of order $\mathcal{O}(\sqrt{\Delta t})$ and thus do not contribute to the sum in the limit $\Delta t \rightarrow 0$.

When expanding the squared terms, many cancellations occur. Taking the natural logarithm of Eq. (B13) then leads to the following result for the entropy production Σ along the path:

$$\Sigma(t_f) \equiv \ln \left[\frac{\mathbb{P}[\{\mathbf{r}_i^k\}|\{\mathbf{r}_i^0, \mathbf{r}_i^1\}]}{\mathbb{P}[\{\mathbf{r}_i^{R,k}\}|\{\mathbf{r}_i^{R,0}, \mathbf{r}_i^{R,1}\}]} \right] \tag{B14}$$

$$= \frac{1}{2} \ln \left[\frac{T(\bar{\mathbf{r}}_i^{M-1})T(\bar{\mathbf{r}}_i^{M-2})}{T(\bar{\mathbf{r}}_i^0)T(\bar{\mathbf{r}}_i^1)} \right] - \left\{ \sum_{i=1}^N \sum_{k=1}^{M-2} \frac{\Delta t}{T(\bar{\mathbf{r}}_i^k)} \frac{\Delta \mathbf{r}_i^k}{\Delta t} \cdot \left[\frac{\Delta \mathbf{r}_i^{k+1} - \Delta \mathbf{r}_i^k}{\Delta t^2} - \sum_{j=1}^N \mathbf{f}_{\text{int}}(\bar{\mathbf{r}}_i^k - \bar{\mathbf{r}}_j^k) \right] \right\} + \mathcal{O}(\sqrt{\Delta t}) \tag{B15}$$

$$\xrightarrow{\Delta t \rightarrow 0} \ln \left[\frac{T(\bar{\mathbf{r}}_i(t_f))}{T(\bar{\mathbf{r}}_i(0))} \right] - \sum_{i=1}^N \int_0^{t_f} dt \frac{\dot{\mathbf{r}}_i}{T(\mathbf{r}_i)} \cdot \left[\ddot{\mathbf{r}}_i - \sum_{j=1}^N \mathbf{f}_{\text{int}}(\mathbf{r}_i - \mathbf{r}_j) \right]. \tag{B16}$$

In Eq. (B15), the $\mathcal{O}(\sqrt{\Delta t})$ term corresponds to the missing $k = 0$ and unmatched $k = M - 1$ terms that appear in the last line of Eq. (B13). They do not contribute in the limit $\Delta t \rightarrow 0$.

The EPR σ is then defined as $\sigma = \lim_{t_f \rightarrow \infty} \frac{\Sigma(t_f)}{t_f}$ and we thus find:

$$\sigma = \sum_{i=1}^N \left\langle \frac{\dot{\mathbf{r}}_i}{T(\mathbf{r}_i)} \cdot \left[\sum_{j=1}^N \mathbf{f}_{\text{int}}(\mathbf{r}_i - \mathbf{r}_j) - \ddot{\mathbf{r}}_i \right] \right\rangle, \tag{B17}$$

where we have assumed the system to be ergodic. In Eq. (8), we then define a fluctuating EPR density $\hat{\sigma}(\mathbf{r})$ such that $\int d^d \mathbf{r} \langle \hat{\sigma}(\mathbf{r}) \rangle = \sigma$.

Appendix C: EPR for PBPs

1. TRS of non-interacting PBPs

It is useful to convert the α -discretized Langevin equation (18) into an equivalent Stratonovich-discretized one. This incurs an extra force $(\alpha - \frac{1}{2}) \nabla T(\mathbf{r})$, and the new Langevin equation is

$$\dot{\mathbf{r}} \stackrel{1/2}{=} \left(\alpha - \frac{1}{2} \right) \nabla T(\mathbf{r}) + \sqrt{2T(\mathbf{r})} \boldsymbol{\eta}. \tag{C1}$$

In discretized form, we may write this as

$$\Delta \mathbf{r}^k = \left(\alpha - \frac{1}{2} \right) \nabla T(\bar{\mathbf{r}}^k) \Delta t + \sqrt{2T(\bar{\mathbf{r}}^k)} \Delta \boldsymbol{\eta}^k. \tag{C2}$$

where we are using $\bar{\mathbf{r}}^k$, the position evaluated at the midpoint of the timestep, as defined in Eq. (B1). We index our timesteps by $k \in \{0, \dots, M\}$, and take starting time $t_0 = 0$ and finishing time $t_M \equiv t_f$.

We know the probability of a noise realization:

$$\mathbb{P}\{\{\Delta\boldsymbol{\eta}^k\}\} = \frac{1}{(2\pi)^{dN/2}} \exp\left[-\frac{1}{2\Delta t} \sum_{k=0}^{M-1} |\Delta\boldsymbol{\eta}^k|^2\right] \quad (\text{C3})$$

and can convert this to a probability for the spatial trajectory using the Jacobian determinant of the associated transformation

$$\mathbb{P}\{\{\mathbf{r}^k\}\} = \mathbb{P}\{\{\Delta\boldsymbol{\eta}^k\}\} \left| \frac{\mathbb{D}\{\{\Delta\boldsymbol{\eta}^k\}\}}{\mathbb{D}\{\{\mathbf{r}^k\}\}} \right| \quad (\text{C4})$$

$$= \mathbb{P}\{\{\Delta\boldsymbol{\eta}^k\}\} \det_{\mu,\nu,k,\ell} \left(\frac{\partial\Delta\eta_\mu^k}{\partial r_\nu^\ell} \right), \quad (\text{C5})$$

where $\mu, \nu \in \{1, \dots, d\}$, $k \in \{0, \dots, M-1\}$, and $\ell \in \{1, \dots, M\}$. The quantity $\det_{\mu,\nu,k,\ell}(\partial\Delta\eta_\mu^k/\partial r_\nu^\ell)$ can be understood as the determinant of the $Md \times Md$ matrix whose $(kd + \mu, \ell d + \nu)$ entry is $\partial\Delta\eta_\mu^k/\partial r_\nu^\ell$.

Note first that $\Delta\boldsymbol{\eta}^k$ only depends directly on \mathbf{r}^k and \mathbf{r}^{k+1} by the relation

$$\Delta\eta_\mu^k(\mathbf{r}^k, \mathbf{r}^{k+1}) = \frac{\Delta r_\mu^k - \Delta t(\alpha - \frac{1}{2})\partial_\mu T(\bar{\mathbf{r}}^k)}{\sqrt{2T(\bar{\mathbf{r}}^k)}}. \quad (\text{C6})$$

If we write the Jacobian matrix in block form, made of $M \times M$ blocks of $d \times d$ matrices, it is block triangular, i.e. there exist $d \times d$ matrices A and B such that

$$\frac{\partial\Delta\eta_\mu^k}{\partial r_\nu^\ell} = \delta^{k,\ell} A_{\mu\nu} + \delta^{k+1,\ell} B_{\mu\nu}. \quad (\text{C7})$$

Consequently, the determinant is given by the product of the determinants of the diagonal blocks. The diagonal blocks consist of k, ℓ such that $\ell = k + 1$ (this is due to the fact that k runs from 0 to $M-1$ while ℓ runs from 1 to M). Their elements are

$$\begin{aligned} \frac{\partial\Delta\eta_\mu^k}{\partial r_\nu^{k+1}} &= \frac{1}{\sqrt{2T}} \left\{ \delta_{\mu\nu} - \frac{\Delta r_\mu^k \partial_\nu T}{4T} \right. \\ &\quad \left. + \frac{\Delta t(\alpha - \frac{1}{2})}{2} \left[\frac{\partial_\mu T \partial_\nu T}{2T} - \partial_\mu \partial_\nu T \right] \right\}, \end{aligned} \quad (\text{C8})$$

where each occurrence of T is evaluated at $\bar{\mathbf{r}}^k$. Note that the diagonal elements ($\mu = \nu$) are $\mathcal{O}(1)$, while off-diagonal elements are $\mathcal{O}(\Delta t^{1/2})$. The off-diagonal elements are thus subleading to diagonal elements, and the determinant is just the product of diagonal elements to leading order. This yields

$$\begin{aligned} \det_{\mu,\nu} \left[\frac{\partial\Delta\eta_\mu^k}{\partial r_\nu^{k+1}} \right] &= \frac{1}{(2T)^{d/2}} \left\{ 1 - \frac{\Delta\mathbf{r}^k \cdot \nabla T}{4T} \right. \\ &\quad \left. + \frac{\Delta t(\alpha - \frac{1}{2})}{2} \left[\frac{|\nabla T|^2}{2T} - \nabla^2 T \right] \right\}. \end{aligned} \quad (\text{C9})$$

Taking the product over k yields the determinant of the entire matrix $\frac{\mathbb{D}\{\{\Delta\boldsymbol{\eta}^k\}\}}{\mathbb{D}\{\{\mathbf{r}^k\}\}}$. Executing this and converting the

product into an exponentiated integral in the $M \rightarrow \infty$ and $\Delta t \rightarrow 0$ limit, we find

$$\begin{aligned} \left| \frac{\mathbb{D}\{\boldsymbol{\eta}(t)\}}{\mathbb{D}\{\mathbf{r}(t)\}} \right| &= \left(\prod_{k=0}^{M-1} \frac{1}{(2T(\bar{\mathbf{r}}^k))^{d/2}} \right) \\ &\quad \times \exp \left[\int_0^{t_f} dt \left\{ -\frac{\dot{\mathbf{r}} \cdot \nabla T(\mathbf{r})}{4T(\mathbf{r})} \right. \right. \\ &\quad \left. \left. + \frac{(\alpha - \frac{1}{2})}{2} \left(\frac{|\nabla T(\mathbf{r})|^2}{2T(\mathbf{r})} - \nabla^2 T(\mathbf{r}) \right) \right\} \right]. \end{aligned} \quad (\text{C10})$$

The noise probability can be re-written by inserting (C6) into (C3), which gives in the continuous-time limit

$$\mathbb{P}\{\boldsymbol{\eta}(t)\} \propto \exp \left[-\int_0^{t_f} dt \frac{|\dot{\mathbf{r}} - (\alpha - \frac{1}{2})\nabla T(\mathbf{r})|^2}{4T(\mathbf{r})} \right]. \quad (\text{C11})$$

Inserting (C10) and (C11) into (C5) gives

$$\begin{aligned} \mathbb{P}\{\mathbf{r}(t)\} &\propto \left(\prod_{k=0}^{M-1} \frac{1}{(2T(\bar{\mathbf{r}}^k))^{d/2}} \right) \\ &\quad \times \exp \left[\int_0^{t_f} dt \left\{ -\frac{|\dot{\mathbf{r}} - (\alpha - \frac{1}{2})\nabla T(\mathbf{r})|^2}{4T(\mathbf{r})} \right. \right. \\ &\quad \left. \left. + \frac{(\alpha - \frac{1}{2})}{2} \left(\frac{|\nabla T(\mathbf{r})|^2}{2T(\mathbf{r})} - \nabla^2 T(\mathbf{r}) \right) - \frac{\dot{\mathbf{r}} \cdot \nabla T(\mathbf{r})}{4T(\mathbf{r})} \right\} \right]. \end{aligned} \quad (\text{C12})$$

This result is used in the main text to prove the time-reversal symmetry of α -discretized OD PBPs.

Note that in the main text, we use the abbreviation

$$\prod_{k=0}^{M-1} \frac{1}{(2T(\bar{\mathbf{r}}^k))^{d/2}} \equiv F(\{\bar{\mathbf{r}}^k\}) \quad (\text{C13})$$

for the time-reversal symmetric function F whose exact form is unimportant. Such prefactors will be common in other calculations (e.g. Sec. IV B 1) and do not impact entropy production or the detailed balance condition because they are equal to their time-reversals.

2. EPR for interacting PBPs

As in the non-interacting case, we re-write the α -discretized Langevin equation as a Stratonovich-discretized dynamics, with an additional force $(\alpha - 1/2)\nabla T(\bar{\mathbf{r}}^k)\Delta t$ (C2). The noise probabilities are identical to the non-interacting case, but, to convert to trajectory probabilities in the N -particle phase space, the Jacobian must now include inter-particle forces. Thus Eq. (C5) becomes

$$\mathbb{P}\{\{\mathbf{r}_k\}\} = \mathbb{P}\{\{\Delta\boldsymbol{\eta}_k\}\} \det_{\mu,\nu,i,j,k,\ell} \left(\frac{\partial\Delta\eta_k^{i,\mu}}{\partial r_\ell^{j,\nu}} \right) \quad (\text{C14})$$

where $i, j \in \{1, \dots, N\}$, $\mu, \nu \in \{1, \dots, d\}$, $k \in \{0, \dots, M-1\}$, and $\ell \in \{1, \dots, M\}$. The noise is determined by rearranging the Langevin equation as in (C6),

and the elements of the Jacobian are found by direct algebra to be

$$\frac{\partial \Delta \eta_k^{i,\mu}}{\partial r_\ell^{j,\nu}} = \frac{\delta^{ij}}{\sqrt{2T(\bar{\mathbf{r}}_k^i)}} \left\{ \delta^{\mu\nu} (\delta_{k+1,\ell} - \delta_{k,\ell}) - \frac{\Delta r_k^{i,\mu} \partial^\nu T(\bar{\mathbf{r}}_k^i)}{4T(\bar{\mathbf{r}}_k^i)} + \Delta t F(\{\bar{\mathbf{r}}_k^i\}) \right\} + \frac{(1 - \delta^{ij})}{\sqrt{2T(\bar{\mathbf{r}}_k^i)}} \Delta t G(\{\bar{\mathbf{r}}_k^i\}). \quad (\text{C15})$$

We have absorbed the rest of the derivative into unspecified functions F, G that depend only on the positions, and are thus even under time-reversal so that they cancel out when taking the ratio with the probability of the time-reverse trajectory. We note that, as in the non-interacting case, terms where $\mu \neq \nu$ or $i \neq j$ are subleading in order of Δt with respect to the diagonal elements. Thus the determinant is found by taking the product of the diagonal terms corresponding to $\mu = \nu$, $i = j$, and $\ell = k + 1$, which yields:

$$\det_{\mu,\nu,i,j,k,\ell} \left(\frac{\partial \Delta \eta_k^{i,\mu}}{\partial r_\ell^{j,\nu}} \right) = H(\{\bar{\mathbf{r}}_k^i\}) \exp \left[- \int_0^{t_f} dt \sum_{i=1}^N \frac{\dot{\mathbf{r}}^i \cdot T(\mathbf{r}^i)}{4T(\mathbf{r}^i)} \right]. \quad (\text{C16})$$

Again, H is a time-reversal symmetric term that will play no role in the following. Meanwhile, the noise probability can be rewritten in terms of spatial trajectories as

$$\mathbb{P}[\{\mathbf{r}^i(t)\}] \propto \exp \left[- \int_0^{t_f} dt \sum_{i=1}^N \frac{1}{4T(\mathbf{r}^i)} \times \left| \dot{\mathbf{r}}^i - \left(\alpha - \frac{1}{2} \right)^2 \nabla T(\mathbf{r}^i) - \sum_{j=1}^N \mathbf{f}_{\text{int}}(\mathbf{r}^i - \mathbf{r}^j) \right|^2 \right] \quad (\text{C17})$$

and the path probability is thus given by

$$\mathbb{P}[\{\mathbf{r}^i(t)\}] = K(\{\bar{\mathbf{r}}_k^i, |\Delta \mathbf{r}_k^i|^2\}) \exp \left[- \int_0^{t_f} dt \sum_i \left\{ \frac{\dot{\mathbf{r}}^i \cdot T(\mathbf{r}^i)}{4T(\mathbf{r}^i)} - \frac{\dot{\mathbf{r}}^i \cdot \left[\left(\alpha - \frac{1}{2} \right) \nabla T(\mathbf{r}^i) + \sum_j \mathbf{f}_{\text{int}}(\mathbf{r}^i - \mathbf{r}^j) \right]}{2T(\mathbf{r}^i)} \right\} \right] \quad (\text{C18})$$

where, again, we have absorbed the time-reversal symmetric factors into an unspecified function K .

Appendix D: Exact solution for non-interacting 1d RTPs

Consider non-interacting RTPs in 1 dimension in an activity landscape $v(x)$ and force field $f(x)$, which may or may not be the gradient of a potential. Define the left- and right-moving densities $R(x, t)$ and $L(x, t)$, velocities $v_R = v(x) + f(x)$ and $v_L = v(x) - f(x)$. The equations of motion can then be written as

$$\dot{R} = -\partial_x [v_R R] - \frac{\alpha}{2} R + \frac{\alpha}{2} L \quad (\text{D1})$$

$$\dot{L} = \partial_x [v_L L] + \frac{\alpha}{2} R - \frac{\alpha}{2} L. \quad (\text{D2})$$

The probability density can be written as $\rho = R + L$, the magnetization as $m = R - L$, and the current as $J = v_R R - v_L L$.

To determine the steady-state current and density profile, we use $\dot{\rho} = \dot{J} = 0$ and re-arrange the Master equation in the spirit of what was done in [12, 40]. In the following calculation, we use $J' = -\dot{\rho} = 0$ and the identity $R - L = (J - f\rho)/v$. The steady-state condition for the current reads

$$0 = \dot{J} = v_R \dot{R} - v_L \dot{L} = -[v_R (v_R R)' + v_L (v_L L)'] - \frac{\alpha}{2} [v_R (R - L) + v_L (R - L)] \quad (\text{D3})$$

$$= -\{v_R^2 R' + v_L^2 L' + v_R v_R' R + v_L v_L' L\} - \frac{\alpha}{2} (v_R + v_L) (R - L) \quad (\text{D4})$$

$$= -\left\{ (v^2 + f^2) \rho' + (v v' + f f') \rho + (v f' + f v') (R - L) + 2v f (R - L)' \right\} - \frac{\alpha}{2} 2v \left(\frac{J - f\rho}{v} \right) \quad (\text{D5})$$

$$= -\left\{ [(v^2 + f^2) \rho]' - \frac{1}{2} (v^2 + f^2)' \rho + f' (J - f\rho) - \frac{v' f}{v} (J - f\rho) - 2f (f\rho)' \right\} - \alpha (J - f\rho) \quad (\text{D6})$$

$$= -\left\{ [(v^2 - f^2) \rho]' - \frac{1}{2} (v^2)' \rho + \frac{f^2 v'}{v} \rho + J \left(f' - \frac{v' f}{v} \right) \right\} - \alpha (J - f\rho) \quad (\text{D7})$$

which we can solve for J to find

$$J = \frac{\left\{ \left[\left(\frac{f^2}{\alpha} - \frac{v^2}{\alpha} \right) \rho \right]' + \rho \left(f + \frac{(v^2)'}{2\alpha} - f^2 \frac{v'}{v\alpha} \right) \right\}}{1 - \frac{v' f}{v\alpha} + \frac{f'}{\alpha}}. \quad (\text{D8})$$

One can immediately see the similarities between Eqs. (D8) and (41), which describes the current for a PBP in an inhomogeneous medium (Sec. III D 1). We

can thus read off the effective fields

$$\mu_{\text{eff}} = \frac{1}{1 - \frac{v'f}{v\alpha} + \frac{f'}{\alpha}}, \quad (\text{D9})$$

$$F_{\text{eff}} = f + \frac{(v^2)'}{2\alpha} - f^2 \frac{v'}{v\alpha}, \quad (\text{D10})$$

$$T_{\text{eff}} = \frac{v^2}{\alpha} - \frac{f^2}{\alpha}. \quad (\text{D11})$$

Solving for the steady-state density and current for this

system amounts to plugging μ_{eff} , F_{eff} , and T_{eff} into Eqs. (42), (43), and (44). The pseudo potential is then given by:

$$\Phi(x) = \int_0^x du \frac{\frac{f(u)^2 v'(u)}{v(u)} - \alpha f(u) - v'(u)v(u)}{v(u)^2 - f(u)^2}, \quad (\text{D12})$$

while the density and current read

$$\rho(x) = \frac{e^{-\Phi(x)}}{v(x)^2 - f(x)^2} \alpha \left[\rho(0) \left(\frac{v(0)^2}{\alpha} - \frac{f(0)^2}{\alpha} \right) - J \int_0^x e^{\Phi(u)} \left(1 - \frac{v'(u)f(u)}{v(u)\alpha} + \frac{f'(u)}{\alpha} \right) du \right], \quad (\text{D13})$$

$$J = \frac{1 - e^{\Phi(L)}}{\int_0^L dx \frac{\alpha}{v(x)^2 - f(x)^2} \int_0^L dx' \left(1 - \frac{v'(x')f(x')}{v(x')\alpha} + \frac{f'(x')}{\alpha} \right) e^{\Phi(x') - \Phi(x)} [1 + \Theta(x - x') (e^{\Phi(L)} - 1)]}. \quad (\text{D14})$$

If $f(x) = 0$, we see that $\Phi(x) = -\ln \left[\frac{v(x)}{v(0)} \right]$ and therefore $\Phi(L) = 0$ and $J = 0$.

If $f(x) \neq 0$ but $v(x)$ is a constant v_0 (a case that has received considerable attention, e.g. in [12, 29, 70]), the condition to have a nonzero current reads

$$0 \neq -\Phi(L) = \frac{\alpha}{v_0^2} \int_0^L dx \frac{\tilde{f}(x)}{1 - \tilde{f}(x)^2}, \quad (\text{D15})$$

where $\tilde{f}(x) = f(x)/v_0$. The sign of J is the same as the sign of $-\Phi(L)$, which is helpful to determine the sign of the current for RTPs in complex potential landscapes, e.g. in quenched random potentials. Note that in regions where $\tilde{f}(x) < 1$ the particles are unable to move in the direction opposite to f , and can be trapped in a potential minimum. The solution doesn't apply to systems where such losses of ergodicity occur.

In the general case where $f(x)$ and $v(x)$ vary spatially, as originally studied for ABPs in [18], the condition for a finite ratchet current—namely, the aperiodicity of $\Phi(x)$ in Eq. (D12)—specifies the joint condition for $V(x)$ and $v(x)$ to induce a current.

This exact solution agrees with numerical particle-based simulations, as demonstrated in Fig. 8.

Appendix E: EPR of interacting AOUPs in activity landscapes

Here we detail the calculation of the EPR for interacting AOUPs in an activity landscape given in Eq. (112). This calculation is quite similar to that of U-PBPs given in Sec. B; however, there are important differences, and we will thus detail it separately here. As for U-PBPs, although the AOUP dynamics (109)-(110) suffer no discretization ambiguity, it is necessary to use caution

when calculating path probabilities. Thus we consider a Stratonovich-discretized version of the dynamics, using $\bar{\mathbf{r}}_i^k$, the position evaluated at the midpoint of the k th timestep, as defined in Eq. (B1), and the spatial increments $\Delta \mathbf{r}_i^k$ as defined in Eq. (B2). We thus find the discretized dynamics:

$$\begin{aligned} \tau \left(\frac{\Delta \mathbf{r}_i^{k+1} - \mathbf{r}_i^k}{\Delta t^2} \right) &= -\frac{\Delta \mathbf{r}_i^k}{\Delta t} + \sqrt{2D(\bar{\mathbf{r}}_i^k)} \Delta \boldsymbol{\eta}_i^{k+1} \quad (\text{E1}) \\ &+ \sum_j \left[1 + \tau \left(\frac{\Delta \mathbf{r}_i^k}{\Delta t} - \frac{\Delta \mathbf{r}_j^k}{\Delta t} \right) \cdot \nabla \right] \mathbf{f}_{\text{int}}(\bar{\mathbf{r}}_i^k - \bar{\mathbf{r}}_j^k) \end{aligned}$$

where $\Delta \boldsymbol{\eta}_i^{k+1}$ is a centered Gaussian noise that satisfies $\langle \Delta \boldsymbol{\eta}_{i,\mu}^k \Delta \boldsymbol{\eta}_{j,\nu}^k \rangle = \delta_{ij} \delta_{\mu\nu} \delta_{k\ell} / \Delta t$. We know the probability of a realization of this noise to be given by

$$\mathbb{P}[\{\Delta \boldsymbol{\eta}_i^k\} | \{\mathbf{r}_i^0, \mathbf{r}_i^1\}] \propto \exp \left[-\sum_{i=1}^N \sum_{k=1}^{M-1} \frac{\Delta t}{2} |\Delta \boldsymbol{\eta}_i^k|^2 \right], \quad (\text{E2})$$

which can be used to find the probability of a spatial trajectory, using the relation

$$\mathbb{P}[\{\mathbf{r}_i^k\} | \{\mathbf{r}_i^0, \mathbf{r}_i^1\}] = \mathbb{P}[\{\Delta \boldsymbol{\eta}_i^k\} | \{\mathbf{r}_i^0, \mathbf{r}_i^1\}] \left| \frac{\mathbb{D}[\{\Delta \boldsymbol{\eta}_i^k\} | \{\mathbf{r}_i^0, \mathbf{r}_i^1\}]}{\mathbb{D}[\{\mathbf{r}_i^k\} | \{\mathbf{r}_i^0, \mathbf{r}_i^1\}]} \right|. \quad (\text{E3})$$

Here, $|\mathbb{D}[\{\Delta \boldsymbol{\eta}_i^k\} | \{\mathbf{r}_i^0, \mathbf{r}_i^1\}] / \mathbb{D}[\{\mathbf{r}_i^k\} | \{\mathbf{r}_i^0, \mathbf{r}_i^1\}]|$ is the Jacobian between the $M-1$ variables $\{\Delta \boldsymbol{\eta}_i^k\}_{k=1}^{M-1}$ and the $M-1$ variables $\{\mathbf{r}_i^k\}_{k=2}^M$. Note the shift in k indices: $\Delta \boldsymbol{\eta}_i^k$ determines \mathbf{r}_i^{k+1} . Note that we condition on the positions in the first two timesteps, $\{\mathbf{r}_i^0, \mathbf{r}_i^1\}$, which is equivalent to conditioning on the initial positions and momenta. We first note, using the relation between the variables given by Eq. (E1), that this Jacobian will be upper triangular

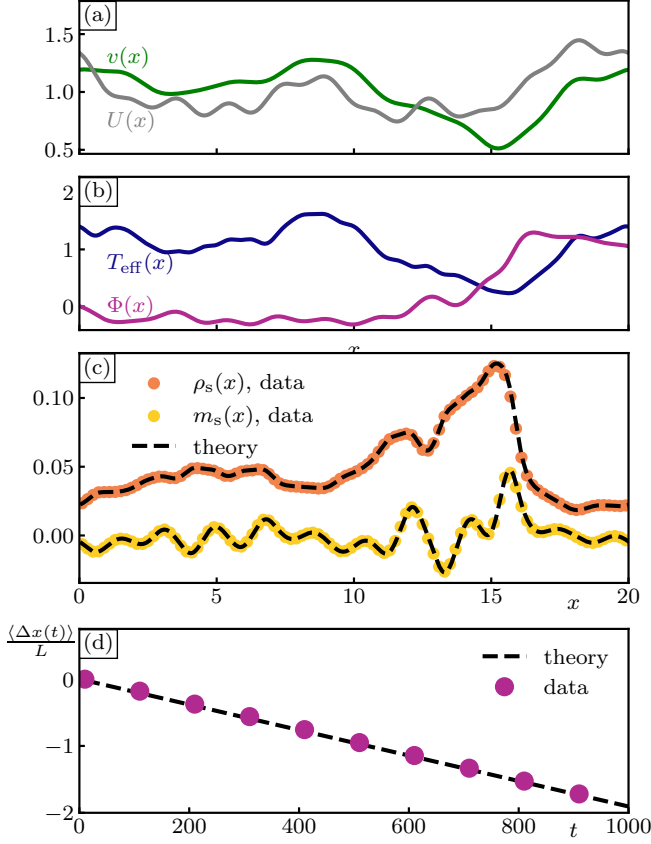


FIG. 8. **Particle simulations of non-interacting RTPs in $d = 1$.** (a) The activity and potential landscapes are given by $v(x)$ and $U(x)$, respectively. (b) The effective temperature $T_{\text{eff}}(x)$ and pseudo-potential $\Phi(x)$, as defined in Eqs. (D11) and (D12). (c) Particle density ρ and polarization m , along with the exact solution (black), whose explicit form for ρ is written in Eq. (D13). (d) Average particle displacement over time (points), along with the theoretical prediction (line) given in Eq. (D14).

in the time dimension, because

$$\frac{\partial \Delta \eta_{i,\mu}^{k+1}}{\partial r_{j,\nu}^\ell} = 0 \text{ whenever } \ell > k + 2. \quad (\text{E4})$$

For the diagonal elements $\partial \Delta \eta_{i,\mu}^{k+1} / \partial r_{j,\nu}^{k+2}$, we have

$$\frac{\delta_{ij} \delta_{\mu\nu} \tau}{\Delta t^2} = \sqrt{2D(\bar{\mathbf{r}}_i^k)} \frac{\partial \Delta \eta_{i,\mu}^{k+1}}{\partial r_{j,\nu}^{k+2}} \quad (\text{E5})$$

from which we find the determinant

$$\left| \frac{\mathbb{D}[\{\Delta \boldsymbol{\eta}_i^k\} | \{\mathbf{r}_i^0, \mathbf{r}_i^1\}]}{\mathbb{D}[\{\mathbf{r}_i^k\} | \{\mathbf{r}_i^0, \mathbf{r}_i^1\}]} \right| = \prod_{k=0}^{M-2} \prod_{i=1}^N \frac{\tau}{\Delta t^2 \sqrt{2D(\bar{\mathbf{r}}_i^k)}} \quad (\text{E6})$$

$$\propto \prod_{k=0}^{M-2} \prod_{i=1}^N \frac{1}{\sqrt{D(\bar{\mathbf{r}}_i^k)}}. \quad (\text{E7})$$

Next, we convert the noise probability [Eq. (E2)] into spatial coordinates using Eq. (E1):

$$\begin{aligned} & \mathbb{P}[\{\Delta \boldsymbol{\eta}_i^k\} | \{\mathbf{r}_i^0, \mathbf{r}_i^1\}] \quad (\text{E8}) \\ & \propto \exp \left[- \sum_{i=1}^N \sum_{k=0}^{M-2} \frac{\Delta t}{4D(\bar{\mathbf{r}}_i^k)} \tau \left(\frac{\Delta \mathbf{r}_i^{k+1} - \Delta \mathbf{r}_i^k}{\Delta t^2} \right) \right. \\ & \quad \left. + \frac{\Delta \mathbf{r}_i^k}{\Delta t} - \sum_{j=1}^N \left[1 + \tau \left(\frac{\Delta \mathbf{r}_i^k}{\Delta t} - \frac{\Delta \mathbf{r}_j^k}{\Delta t} \right) \cdot \nabla \right] \mathbf{f}_{\text{int}}(\bar{\mathbf{r}}_i^k - \bar{\mathbf{r}}_j^k) \right]^2. \end{aligned}$$

Equations (E3), (E6), and (E8) give the trajectory probability density. Once again defining a trajectory's time-reverse as $\mathbf{r}_i^{R,k} \equiv \mathbf{r}_i^{M-k}$, we find the ratio between the forward and reverse trajectory probabilities to be

$$\begin{aligned} & \frac{\mathbb{P}[\{\mathbf{r}_i^k\} | \{\mathbf{r}_i^0, \mathbf{r}_i^1\}]}{\mathbb{P}[\{\mathbf{r}_i^{R,k}\} | \{\mathbf{r}_i^{R,0}, \mathbf{r}_i^{R,1}\}]} \\ & = \sqrt{\frac{D(\bar{\mathbf{r}}_i^{M-1})D(\bar{\mathbf{r}}_i^{M-2})}{D(\bar{\mathbf{r}}_i^0)D(\bar{\mathbf{r}}_i^1)}} \exp \left[- \sum_{i=1}^N \sum_{k=0}^{M-2} \frac{\Delta t}{4} \left\{ \frac{1}{D(\bar{\mathbf{r}}_i^k)} \tau \frac{\Delta \mathbf{r}_i^{k+1} - \Delta \mathbf{r}_i^k}{\Delta t^2} + \frac{\Delta \mathbf{r}_i^k}{\Delta t} - \sum_{j=1}^N \left[1 + \tau \left(\frac{\Delta \mathbf{r}_i^k}{\Delta t} - \frac{\Delta \mathbf{r}_j^k}{\Delta t} \right) \cdot \nabla \right] \mathbf{f}_{\text{int}}(\bar{\mathbf{r}}_i^k - \bar{\mathbf{r}}_j^k) \right\}^2 \right. \\ & \quad \left. - \frac{1}{D(\bar{\mathbf{r}}_i^{M-k-1})} \tau \frac{\Delta \mathbf{r}_i^{M-k-1} - \Delta \mathbf{r}_i^{M-k-2}}{\Delta t^2} - \frac{\Delta \mathbf{r}_i^{M-k-1}}{\Delta t} - \sum_{j=1}^N \left[1 - \left(\frac{\Delta \mathbf{r}_i^{M-k-1}}{\Delta t} - \frac{\Delta \mathbf{r}_j^{M-k-1}}{\Delta t} \right) \cdot \nabla \right] \mathbf{f}_{\text{int}}(\bar{\mathbf{r}}_i^{M-k-1} - \bar{\mathbf{r}}_j^{M-k-1}) \right]^2 \Bigg] \\ & = \sqrt{\frac{D(\bar{\mathbf{r}}_i^{M-1})D(\bar{\mathbf{r}}_i^{M-2})}{D(\bar{\mathbf{r}}_i^0)D(\bar{\mathbf{r}}_i^1)}} \exp \left[- \sum_{i=1}^N \sum_{k=0}^{M-2} \frac{\Delta t}{4D(\bar{\mathbf{r}}_i^k)} \tau \frac{\Delta \mathbf{r}_i^{k+1} - \Delta \mathbf{r}_i^k}{\Delta t^2} + \frac{\Delta \mathbf{r}_i^k}{\Delta t} - \sum_{j=1}^N \left[1 + \tau \left(\frac{\Delta \mathbf{r}_i^k}{\Delta t} - \frac{\Delta \mathbf{r}_j^k}{\Delta t} \right) \cdot \nabla \right] \mathbf{f}_{\text{int}}(\bar{\mathbf{r}}_i^k - \bar{\mathbf{r}}_j^k) \right]^2 \\ & \quad + \sum_{i=1}^N \sum_{k=1}^{M-1} \frac{\Delta t}{4D(\bar{\mathbf{r}}_i^k)} \tau \frac{\Delta \mathbf{r}_i^k - \Delta \mathbf{r}_i^{k-1}}{\Delta t^2} - \frac{\Delta \mathbf{r}_i^k}{\Delta t} - \sum_{j=1}^N \left[1 - \tau \left(\frac{\Delta \mathbf{r}_i^k}{\Delta t} - \frac{\Delta \mathbf{r}_j^k}{\Delta t} \right) \cdot \nabla \right] \mathbf{f}_{\text{int}}(\bar{\mathbf{r}}_i^k - \bar{\mathbf{r}}_j^k) \right]^2, \quad (\text{E9}) \end{aligned}$$

where, in the second equality, we have relabelled the time indices for the backward path as $M - k - 1 \rightarrow k$. In the last line of Eq. (E9), we may replace $\frac{\Delta \mathbf{r}_i^{k+1} - \Delta \mathbf{r}_i^k}{\Delta t^2}$ with $\frac{\Delta \mathbf{r}_i^{k+1} - \Delta \mathbf{r}_i^k}{\Delta t^2}$, since their difference is of order $\mathcal{O}(\sqrt{\Delta t})$ and

thus do not contribute to the sum in the limit $\Delta t \rightarrow 0$. Taking the natural logarithm of Eq. (E9) then leads to the following result for the entropy production Σ along the path:

$$\Sigma(t_f) \equiv \ln \left[\frac{\mathbb{P}[\{\mathbf{r}_i^k\} | \{\mathbf{r}_i^0, \mathbf{r}_i^1\}]}{\mathbb{P}[\{\mathbf{r}_i^{R,k}\} | \{\mathbf{r}_i^{R,0}, \mathbf{r}_i^{R,1}\}]} \right] \quad (\text{E10})$$

$$\begin{aligned} &= - \left\{ \sum_{i=1}^N \sum_{k=1}^{M-2} \frac{\Delta t}{D(\bar{\mathbf{r}}_i^k)} \left[\tau \frac{\Delta \mathbf{r}_i^{k+1} - \Delta \mathbf{r}_i^k}{\Delta t^2} - \sum_{j=1}^N \mathbf{f}_{\text{int}}(\bar{\mathbf{r}}_i^k - \bar{\mathbf{r}}_j^k) \right] \cdot \left[\frac{\Delta \mathbf{r}_i^k}{\Delta t} - \tau \sum_{j=1}^N \left(\frac{\Delta \mathbf{r}_i^k}{\Delta t} - \frac{\Delta \mathbf{r}_j^k}{\Delta t} \right) \cdot \nabla \mathbf{f}_{\text{int}}(\bar{\mathbf{r}}_i^k - \bar{\mathbf{r}}_j^k) \right] \right\} \\ &\quad + \frac{1}{2} \ln \left[\frac{D(\bar{\mathbf{r}}_i^{M-1}) D(\bar{\mathbf{r}}_i^{M-2})}{D(\bar{\mathbf{r}}_i^0) D(\bar{\mathbf{r}}_i^1)} \right] + \mathcal{O}(\sqrt{\Delta t}) \\ &\xrightarrow{\Delta t \rightarrow 0} - \sum_{i=1}^N \int_0^{t_f} dt \frac{1}{D(\mathbf{r}_i)} \left[\tau \ddot{\mathbf{r}}_i - \sum_{j=1}^N \mathbf{f}_{\text{int}}(\mathbf{r}_i - \mathbf{r}_j) \right] \cdot \left[\dot{\mathbf{r}}_i - \tau \sum_{j=1}^N (\dot{\mathbf{r}}_i - \dot{\mathbf{r}}_j) \cdot \nabla \mathbf{f}_{\text{int}}(\mathbf{r}_i - \mathbf{r}_j) \right] + \ln \left[\frac{D(\bar{\mathbf{r}}_i(t_f))}{D(\bar{\mathbf{r}}_i(0))} \right]. \quad (\text{E11}) \end{aligned}$$

In Eq. (E11), the $\mathcal{O}(\sqrt{\Delta t})$ term corresponds to the missing $k = 0$ and unmatched $k = M - 1$ terms that appear in the last line of Eq. (E9). They do not contribute in the limit $\Delta t \rightarrow 0$. The EPR σ is then defined as

$\sigma = \lim_{t_f \rightarrow \infty} \frac{\Sigma(t_f)}{t_f}$ and we thus find:

$$\begin{aligned} \sigma &= \sum_{i=1}^N \left\langle \frac{1}{D(\mathbf{r}_i)} \left[\sum_{j=1}^N \mathbf{f}_{\text{int}}(\mathbf{r}_i - \mathbf{r}_j) - \tau \ddot{\mathbf{r}}_i \right] \cdot \left[\dot{\mathbf{r}}_i - \tau \sum_{j=1}^N (\dot{\mathbf{r}}_i - \dot{\mathbf{r}}_j) \cdot \nabla \mathbf{f}_{\text{int}}(\mathbf{r}_i - \mathbf{r}_j) \right] \right\rangle, \quad (\text{E12}) \end{aligned}$$

where we have assumed the system to be ergodic. In Eq. (112), we then define a fluctuating EPR density $\hat{\sigma}(\mathbf{r})$ such that $\int d^d \mathbf{r} \langle \hat{\sigma}(\mathbf{r}) \rangle = \sigma$. The term proportional to τ in Eq. (E12) is specific to AOUPs and distinguishes their EPR from that of U-PBPs.

-
- [1] L. Berthier and J. Kurchan, Active systems, in *Active Matter and Nonequilibrium Statistical Physics*, Les Houches, Vol. CXII, edited by G. Gompper, M. Marchetti, J. Tailleur, J. Yeomans, and C. Salomon (Oxford University Press, 2022).
 - [2] P. Reimann, Brownian motors: noisy transport far from equilibrium, *Physics Reports* **361**, 57 (2002).
 - [3] J. M. Parrondo and P. Español, Criticism of feynman's analysis of the ratchet as an engine, *American Journal of Physics* **64**, 1125 (1996).
 - [4] A. Ajdari and J. Prost, Mouvement induit par un potentiel periodique de basse symmetrie: dielectrophorese pulsee, *Comptes rendus de l'Académie des Sciences II*, 1635 (1992).
 - [5] J. Rousselet, L. Salome, A. Ajdari, and J. Prost, Directional motion of brownian particles induced by a periodic asymmetric potential, *Nature* **370**, 446 (1994), number: 6489 Publisher: Nature Publishing Group.
 - [6] A. Ajdari, D. Mukamel, L. Peliti, and J. Prost, Rectified motion induced by ac forces in periodic structures, *Journal de Physique I* **4**, 1551 (1994), publisher: EDP Sciences.
 - [7] F. Jülicher, A. Ajdari, and J. Prost, Modeling molecular motors, *Reviews of Modern Physics* **69**, 1269 (1997).
 - [8] E. Frey and K. Kroy, Brownian motion: a paradigm of soft matter and biological physics, *Annalen der Physik* **517**, 20 (2005).
 - [9] O. Campas, Y. Kafri, K. Zeldovich, J. Casademunt, and J.-F. Joanny, Collective dynamics of interacting molecular motors, *Physical review letters* **97**, 038101 (2006).
 - [10] P. Hänggi and F. Marchesoni, Artificial Brownian motors: Controlling transport on the nanoscale, *Reviews of Modern Physics* **81**, 387 (2009), publisher: American Physical Society.
 - [11] P. Galajda, J. Keymer, P. Chaikin, and R. Austin, A Wall of Funnels Concentrates Swimming Bacteria, *Journal of Bacteriology* **189**, 8704 (2007), publisher: American Society for Microbiology.

- [12] L. Angelani, A. Costanzo, and R. D. Leonardo, Active ratchets, *EPL (Europhysics Letters)* **96**, 68002 (2011), publisher: IOP Publishing.
- [13] R. Di Leonardo, L. Angelani, D. Dell'Arciprete, G. Ruocco, V. Iebba, S. Schippa, M. P. Conte, F. Mearini, F. De Angelis, and E. Di Fabrizio, Bacterial ratchet motors, *Proceedings of the National Academy of Sciences* **107**, 9541 (2010).
- [14] A. Sokolov, M. M. Apodaca, B. A. Grzybowski, and I. S. Aranson, Swimming bacteria power microscopic gears, *Proceedings of the National Academy of Sciences* **107**, 969 (2010).
- [15] M. O. Magnasco, Forced thermal ratchets, *Physical Review Letters* **71**, 1477 (1993), publisher: American Physical Society.
- [16] M. O. Magnasco, Molecular combustion motors, *Physical Review Letters* **72**, 2656 (1994), publisher: American Physical Society.
- [17] A. Fiasconaro, W. Ebeling, and E. Gudowska-Nowak, Active Brownian motion models and applications to ratchets, *The European Physical Journal B* **65**, 403 (2008).
- [18] A. Pototsky, A. M. Hahn, and H. Stark, Rectification of self-propelled particles by symmetric barriers, *Physical Review E, Statistical, Nonlinear, and Soft Matter Physics* **87**, 042124 (2013).
- [19] P. K. Ghosh, V. R. Misko, F. Marchesoni, and F. Nori, Self-propelled janus particles in a ratchet: Numerical simulations, *Physical review letters* **110**, 268301 (2013).
- [20] L. M. Lopatina, C. Reichhardt, and C. J. O. Reichhardt, Self-driven particles on asymmetric trap arrays, in *Optical Trapping and Optical Micromanipulation X*, Vol. 8810 (SPIE, 2013) pp. 129–139.
- [21] B.-q. Ai, Q.-y. Chen, Y.-f. He, F.-g. Li, and W.-r. Zhong, Rectification and diffusion of self-propelled particles in a two-dimensional corrugated channel, *Physical Review E* **88**, 062129 (2013), publisher: American Physical Society.
- [22] C. Reichhardt and C. J. O. Reichhardt, Active matter ratchets with an external drift, *Physical Review E* **88**, 062310 (2013), publisher: American Physical Society.
- [23] N. Koumakis, C. Maggi, and R. D. Leonardo, Directed transport of active particles over asymmetric energy barriers, *Soft Matter* **10**, 5695 (2014), publisher: The Royal Society of Chemistry.
- [24] E. Yariv and O. Schnitzer, Ratcheting of Brownian swimmers in periodically corrugated channels: A reduced Fokker-Planck approach, *Physical Review E* **90**, 032115 (2014).
- [25] B. Bijnens and C. Maes, Pushing run-and-tumble particles through a rugged channel, *Journal of Statistical Mechanics: Theory and Experiment* **2021**, 033206 (2021), publisher: IOP Publishing and SISSA.
- [26] D. Martin and T. A. d. Pirey, AOUP in the presence of Brownian noise: a perturbative approach, *Journal of Statistical Mechanics: Theory and Experiment* **2021**, 043205 (2021), publisher: IOP Publishing.
- [27] J. O'Byrne, Y. Kafri, J. Tailleur, and F. van Wijland, Time irreversibility in active matter, from micro to macro, *Nature Reviews Physics* **4**, 167 (2022), number: 3 Publisher: Nature Publishing Group.
- [28] J.-F. Derivaux, R. L. Jack, and M. E. Cates, Rectification in a mixture of active and passive particles subject to a ratchet potential, *Journal of Statistical Mechanics: Theory and Experiment* **2022**, 043203 (2022).
- [29] Z. Zhen and G. Pruessner, *Optimal Ratchet Potentials for Run-and-Tumble particles* (2022), arXiv:2204.04070 [cond-mat].
- [30] N. Khatri and R. Kapral, Inertial effects on rectification and diffusion of active Brownian particles in an asymmetric channel, *The Journal of Chemical Physics* **158**, 124903 (2023), arXiv:2301.02902 [cond-mat, physics:physics].
- [31] M. Muhsin and M. Sahoo, Inertial active ratchet: Simulation versus theory, *Physical Review E* **107**, 054601 (2023), publisher: American Physical Society.
- [32] M. Rojas-Vega, P. de Castro, and R. Soto, Mixtures of self-propelled particles interacting with asymmetric obstacles, *The European Physical Journal E* **46**, 95 (2023).
- [33] A. Ryabov and M. Tasinkevych, Mechanochemical active ratchet, *Scientific Reports* **13**, 20572 (2023), publisher: Nature Publishing Group.
- [34] C. D. Schimming, C. J. O. Reichhardt, and C. Reichhardt, Active nematic ratchet in asymmetric obstacle arrays, *Physical Review E* **109**, 064602 (2024), publisher: American Physical Society.
- [35] S. Anand, X. Ma, S. Guo, S. Martiniani, and X. Cheng, Transport and energetics of bacterial rectification, *Proceedings of the National Academy of Sciences* **121**, e2411608121 (2024), <https://www.pnas.org/doi/pdf/10.1073/pnas.2411608121>.
- [36] C. Wang, W. Lian, H. Li, W. Tian, and K. Chen, Spontaneous unidirectional rotation of a symmetric gear driven by spherical active particles, *National Science Open* **3**, 20230066 (2024), number: 4 Publisher: China Science Publishing & Media Ltd. and EDP Sciences.
- [37] N. G. Van Kampen, Diffusion in inhomogeneous media, *Journal of Physics and Chemistry of Solids* **49**, 673 (1988).
- [38] N. G. van Kampen, Relative stability in nonuniform temperature, *IBM Journal of Research and Development* **32**, 107 (1988), conference Name: IBM Journal of Research and Development.
- [39] M. J. Schnitzer, Theory of continuum random walks and application to chemotaxis, *Physical Review E* **48**, 2553 (1993), publisher: American Physical Society.
- [40] J. Tailleur and M. E. Cates, Statistical Mechanics of Interacting Run-and-Tumble Bacteria, *Physical Review Letters* **100**, 218103 (2008).
- [41] M. E. Cates and J. Tailleur, When are active Brownian particles and run-and-tumble particles equivalent? Consequences for motility-induced phase separation, *EPL* **101**, 20010 (2013).
- [42] J. Stenhammar, R. Wittkowski, D. Marenduzzo, and M. E. Cates, Light-induced self-assembly of active rectification devices, *Science Advances* **2**, e1501850 (2016), publisher: American Association for the Advancement of Science.
- [43] C. Rein, M. Kolář, K. Kroy, and V. Holubec, Force-free and autonomous active Brownian ratchets ^(a), *Europhysics Letters* **142**, 31001 (2023).
- [44] J. Metzger, S. Ro, and J. Tailleur, Exceptions to the ratchet principle: When hidden symmetries prevent steady currents, *arxiv preprint arxiv:2412.07851* (2024).
- [45] D. S. Dean, Langevin equation for the density of a system of interacting Langevin processes, *Journal of Physics A: Mathematical and General* **29**, L613 (1996).
- [46] A. Celani, S. Bo, R. Eichhorn, and E. Aurell, Anomalous Thermodynamics at the Microscale, *Phys. Rev. Lett.*

- 109**, 260603 (2012).
- [47] J. Irving and J. G. Kirkwood, The statistical mechanical theory of transport processes. iv. the equations of hydrodynamics, *The Journal of chemical physics* **18**, 817 (1950).
- [48] T. Frankel, *The geometry of physics: an introduction* (Cambridge university press, 2011).
- [49] T. A. de Pirey, L. F. Cugliandolo, V. Lecomte, and F. van Wijland, Path integrals and stochastic calculus, *Advances in Physics* **71**, 1 (2022), arXiv:2211.09470 [cond-mat, physics:math-ph].
- [50] H. Risken, Solutions of the fokker-planck equation in detailed balance, *Zeitschrift für Physik A Hadrons and nuclei* **251**, 231 (1972).
- [51] H. Risken, *The Fokker-Planck Equation: Methods of Solution and Applications*, edited by H. Haken, Springer Series in Synergetics, Vol. 18 (Springer, Berlin, Heidelberg, 1996).
- [52] C. Gardiner, *Stochastic methods*, Vol. 4 (Springer Berlin Heidelberg, 2009).
- [53] M. E. Cates and J. Tailleur, Motility-Induced Phase Separation, *Annual Review of Condensed Matter Physics* **6**, 219 (2015).
- [54] J. Arlt, V. A. Martinez, A. Dawson, T. Pilizota, and W. C. K. Poon, Painting with light-powered bacteria, *Nature Communications* **9**, 768 (2018), publisher: Nature Publishing Group.
- [55] G. Frangipane, D. Dell'Arciprete, S. Petracchini, C. Maggi, F. Saglimbeni, S. Bianchi, G. Vizsnyiczai, M. L. Bernardini, and R. Di Leonardo, Dynamic density shaping of photokinetic E. coli, *eLife* **7**, e36608 (2018), publisher: eLife Sciences Publications, Ltd.
- [56] N. Razin, Entropy production of an active particle in a box, *Physical Review E* **102**, 030103 (2020).
- [57] L. Cocconi, R. Garcia-Millan, Z. Zhen, B. Buturca, and G. Pruessner, Entropy production in exactly solvable systems, *Entropy* **22**, 1252 (2020).
- [58] D. Frydel, Intuitive view of entropy production of ideal run-and-tumble particles, *Physical Review E* **105**, 034113 (2022).
- [59] M. Paoluzzi, A. Puglisi, and L. Angelani, Entropy Production of Run-and-Tumble Particles, *Entropy* **26**, 443 (2024), number: 6 Publisher: Multidisciplinary Digital Publishing Institute.
- [60] É. Fodor, C. Nardini, M. E. Cates, J. Tailleur, P. Visco, and F. van Wijland, How Far from Equilibrium Is Active Matter?, *Physical Review Letters* **117**, 038103 (2016), publisher: American Physical Society.
- [61] S. Ro, B. Guo, A. Shih, T. V. Phan, R. H. Austin, D. Levine, P. M. Chaikin, and S. Martiniani, Model-free measurement of local entropy production and extractable work in active matter, *Phys. Rev. Lett.* **129**, 220601 (2022).
- [62] E. Mallmin, R. A. Blythe, and M. R. Evans, Exact spectral solution of two interacting run-and-tumble particles on a ring lattice, *Journal of Statistical Mechanics: Theory and Experiment* **2019**, 013204 (2019).
- [63] A. P. Solon, J. Stenhammar, R. Wittkowski, M. Kardar, Y. Kafri, M. E. Cates, and J. Tailleur, Pressure and Phase Equilibria in Interacting Active Brownian Spheres, *Physical Review Letters* **114**, 198301 (2015), arXiv:1412.5475 [cond-mat].
- [64] A. P. Solon, J. Stenhammar, M. E. Cates, Y. Kafri, and J. Tailleur, Generalized thermodynamics of phase equilibria in scalar active matter, *Physical Review E* **97**, 020602 (2018).
- [65] A. P. Solon, J. Stenhammar, M. E. Cates, Y. Kafri, and J. Tailleur, Generalized thermodynamics of motility-induced phase separation: phase equilibria, laplace pressure, and change of ensembles, *New Journal of Physics* **20**, 075001 (2018).
- [66] T. Speck, Coexistence of active brownian disks: Van der waals theory and analytical results, *Physical Review E* **103**, 012607 (2021).
- [67] A. Wysocki, A. K. Dasanna, and H. Rieger, Interacting particles in an activity landscape, *New Journal of Physics* **24**, 093013 (2022), publisher: IOP Publishing.
- [68] A. K. Omar, H. Row, S. A. Mallory, and J. F. Brady, Mechanical theory of nonequilibrium coexistence and motility-induced phase separation, *Proceedings of the National Academy of Sciences* **120**, e2219900120 (2023).
- [69] This is a direct consequence of the mapping of non-interacting AOUPs onto the U-PBPs considered in Sec. II B.
- [70] C. Roberts and Z. Zhen, Run-and-tumble motion in a linear ratchet potential: Analytic solution, power extraction, and first-passage properties, *Physical Review E* **108**, 014139 (2023), arXiv:2303.07880 [cond-mat, physics:math-ph, physics:physics].